

A WAVELENGTH-SELECTABLE WDM SOURCE USING A FIBER
SAGNAC LOOP FILTER

A THESIS SUBMITTED TO
THE GRADUATE SCHOOL OF NATURAL AND APPLIED SCIENCES
OF
MIDDLE EAST TECHNICAL UNIVERSITY

BY

ÖZGÜR ERGÜL

IN PARTIAL FULFILLMENT OF THE REQUIREMENT
FOR
THE DEGREE OF MASTER OF SCIENCE
IN
ELECTRICAL AND ELECTRONICS ENGINEERING

SEPTEMBER 2006

Approval of the Graduate School of Natural Sciences

Prof. Dr. Canan ÖZGEN
Director

I certify that this thesis satisfies all the requirements as a thesis for the degree of Master of Science.

Prof. Dr. İsmet ERKMEN
Head of Department

This is to certify that we have read this thesis and that in our opinion it is fully adequate, in scope and quality, as a thesis for the degree of Master of Science.

Prof. Dr. Rüyal ERGÜL
Supervisor

Examining Committee Members

Prof. Dr. Mete Severcan

Prof. Dr. Rüyal Ergül

Prof. Dr. Gönül T. Sayan

Assist. Prof. A. Behzat Şahin

Orhan Şengül (M.S. in EE)

I hereby declare that all information in this document has been obtained and presented in accordance with academic rules and ethical conduct. I also declare that, as required by these rules and conduct, I have fully cited referenced all material and results that are not original to this work.

Name, Last name: Özgür ERGÜL

Signature :

ABSTRACT

A WAVELENGTH-SELECTABLE WDM SOURCE USING A FIBER SAGNAC LOOP FILTER

ERGÜL, Özgür

M.S., Department of Electrical and Electronics Engineering

Supervisor : Prof. Dr. Rüyal ERGÜL

September 2006, 74 pages

The demand for faster data transmission has been increasing since the wide acceptance of the Internet. To meet this ever increasing demand, optical communication systems use Wavelength Division Multiplexing (WDM) to transport more information per fiber by utilizing multiple wavelength channels. Multi-wavelength laser sources are one of the most important components of such WDM systems. In this thesis a multi-wavelength laser source is proposed. A fiber Sagnac loop filter is used to produce a grid pattern with peaks at a certain set of wavelengths. Then any desired channel is chosen from the grid by using an adjustable Fiber Bragg Grating.

Keywords: WDM sources, fiber Sagnac filter, fiber lasers, wavelength selectable lasers

ÖZ

FİBER SAGNAC DÖNGÜ FİLTRESİ KULLANAN DALGABOYU SEÇİLEBİLİR WDM ÜRETEÇ

ERGÜL, Özgür

Y. Lisans, Elektrik ve Elektronik Mühendisliği Bölümü

Tez Yöneticisi: Prof. Dr. Rüyal ERGÜL

Eylül 2006, 74 sayfa

İnternet'in geniş çevrelerce kabulünden bugüne veri iletiminin hızlanması yönündeki talep sürekli artmaktadır. Bu talebi karşılamak için optik haberleşme sistemleri Dalgaboyu Bölmeli Çoklama (Wavelength Division Multiplexing – WDM) yöntemi kullanarak tek bir fiber kablo üzerinden birden fazla dalgaboyunda veri göndermektedir. Bu tür sistemlerin en önemli bileşenlerinden biri de birden fazla dalgaboyunda çalışabilen lazer üreteçlerdir. Bu tezde birden fazla dalgaboyunda çalışabilen bir lazer üreteç önerilmektedir. Fiber Sagnac döngü filtresi kullanılarak birden fazla dalgaboyunda tepe noktaları olan bir frekans şekli elde edilmektedir. Daha sonra dalgaboyu ayarlanabilen bir Fiber Bragg Dizgisi ile istenilen kanal seçilmektedir.

Anahtar Kelimeler: WDM üreteçler, fiber Sagnac filtre, fiber lazerler, dalgaboyu seçilebilen lazerler

To My Family

ACKNOWLEDGMENTS

I would like to express my deepest gratitude to Prof. Dr. R yal ERG L, for his guidance, advice, criticism, encouragement and insight throughout the research and experiment process.

I would also like to thank Assist. Prof. A. Behzat  AH N for his valuable suggestions and support.

Finally I would like to express my deepest gratitude to my family for their love, support and assistance throughout my life.

TABLE of CONTENTS

ABSTRACT	iv
A WAVELENGTH-SELECTABLE WDM SOURCE USING A FIBER SAGNAC LOOP FILTER	iv
ÖZ	v
ACKNOWLEDGMENTS.....	vii
TABLE of CONTENTS.....	viii
LIST of FIGURES	x
CHAPTERS	
1. INTRODUCTION AND BACKGROUND	1
2. POLARIZATION AND MATHEMATICAL TOOLS TO ANALYZE STATE OF POLARIZATION	5
2.1 Polarization	5
2.2 Mathematical tools used to analyze State of Polarization	6
2.2.1 The Stokes parameters.....	6
2.2.2 Mueller Matrices	8
2.2.3 Jones Formalism.....	9
2.2.4 Poincaré Sphere.....	12
3. FIBER LASERS	14
3.1 Optical components that make up the fiber Laser.....	15
3.1.1 Erbium Doped Fiber Amplifiers	16
3.1.2 Birefringence Concept and Polarization Maintaining Fibers	20
3.1.3 Fiber Bragg Gratings	26
3.1.4 Fiber Couplers	27
3.1.5 Optical Isolators and Circulators.....	30
3.1.6 Sagnac Loop Filter	31
4. EXPERIMENTAL SETUP	34

4.1 The Structure of the Source	35
5. CONCLUSION.....	50
APPENDICES	
A. NORMALIZED JONES AND MUELLER VECTORS FOR LIGHT WITH VARIOUS SOP.....	53
B. MUELLER MATRICES FOR VARIOUS POLARIZERS AND RETARDERS	55
C. JONES MATRICES FOR VARIOUS POLARIZERS AND RETARDERS	58
D. RELATIONSHIPS BETWEEN MUELLER AND JONES MATRIX ELEMENTS.....	60
E. OPTICAL SPECTRUM ANALYZER SETUP	62
F. THE SPEC SHEETS OF THE COMPONENTS USED IN THE FIBER LASER SETUP	66
REFERENCES	73

LIST of FIGURES

Figure 1 Wavelength regions for single-mode fiber.....	2
Figure 2 Convention used for Jones formalism - the propagation directions	11
Figure 3 Convention used for Jones formalism - all input & output directions.....	12
Figure 4 Poincaré Sphere	13
Figure 5 There level model of EDF	16
Figure 6 The basic forward pumping scheme for EDFA.....	19
Figure 7 Backward pumping for an EDFA	19
Figure 8 Bi-directional pumping for EDFA.....	20
Figure 9 An illustration of beat length.....	23
Figure 10 Structures of various polarization maintaining fibers	24
Figure 11 Structure of a helical core fiber.....	25
Figure 12 Types of PM fibers.....	25
Figure 13 A fiber coupler formed by bringing the core regions close.....	28
Figure 14 Structure of the fiber Sagnac loop filter	31
Figure 15 Structure of the laser	35
Figure 16 A photograph of the setup	36
Figure 17 Frequency spectrum of the comb filter with doubly clad PM.....	37
Figure 18 Frequency spectrum of the comb filter with the PANDA fiber	37
Figure 19 Output power of the EDFA vs pump current	38
Figure 20 The spectrum of EDFA without any input	39
Figure 21 The self-filtering effect of the closed loop EDFA setup	40
Figure 22 A photograph of the adjustable FBG setup	41
Figure 23 Bent metal sheet and the fiber laid on it.....	42
Figure 24 The metal sheet before and after applying stress.....	43
Figure 25 Relation between the angle and chord length.....	43
Figure 26 The spectrum of the FBGs before and stress is applied.....	45
Figure 27 The spectrum of the FBGs after 5 turns of the screw	46
Figure 28 Single channel output of the source with doubly clad PM.....	47

Figure 29 Dual channel output of the source with doubly clad PM	48
Figure 30 Three wavelength output of the source with doubly clad PM.....	48
Figure 31 Single channel output with PANDA PM	49
Figure 32 Dual channel output with PANDA PM.....	49
Figure 33 A photo of the OSA setup	62
Figure 34 The block diagram of the up/down counter.....	64
Figure 35 A photo of the up/down counter	64

CHAPTER 1

INTRODUCTION AND BACKGROUND

The need for optical fiber communication systems increases as the demand for broadband Internet access increases. Application areas for optical fiber systems are no longer limited to network backbones. Fiber is getting closer to our homes each day. In today's Internet hierarchy optical fiber systems make up the metro networks that interconnect the backbone networks and the local access networks. The use of optical fiber systems in local access networks also increase as *fiber to the premises (FTTP)* technologies find wider acceptance.

The key features that make optical fiber communication systems of choice for today's communication are the very high bandwidth capacity and low-loss characteristics of the fiber. *Wavelength Division Multiplexing (WDM)* systems take advantage of this huge bandwidth by multiplexing several optical carriers at different wavelengths, each modulated with independent high speed data signals, onto the same fiber. Modern systems can handle more than a hundred signals expanding a basic 10Gbit/s fiber optic communication system to a capacity of over 1 Tbit/s over a single fiber pair.

However it wasn't possible to use WDM systems in long distance transmissions until the invention of the *erbium-doped fiber amplifier (EDFA)*. Without an optical amplifier the only way to combat noise for a long distance communication was electronic regeneration. Optical signal had to be demultiplexed, converted to electrical signals, reformed, converted back to optical signals, and re-multiplexed.

The procedure was too cumbersome and the devices involved were too expensive to make WDM a viable technology.

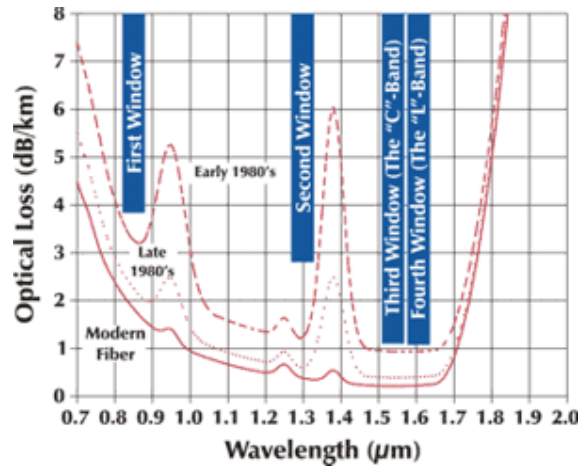


Figure 1 Wavelength regions for single-mode fiber.

An EDFA consists of a short length of fiber doped with erbium, a laser, called the pump laser, operating at 980nm or 1480nm that is used to excite the erbium ions to a higher energy state and a WDM coupler to couple the pump and the signal into the erbium doped fiber. The excited erbium ions decay via stimulated emission as the optical signal with a wavelength around 1550nm passes through the erbium doped fiber, generating a new photon at the same phase and wavelength as the traversing signal. The large bandwidth of EDFA makes it possible to amplify multiple WDM channels simultaneously, independent of the bit rate and data format of each signal. Together with the EDFA, WDM technology has the ability to expand the capacity of a network without having to lay more fiber which makes it system of choice for the telecommunication companies.

WDM systems are divided into two classes. *Coarse Wavelength Division Multiplexing (CWDM)* systems, as their name imply, use coarse channel spacings and utilize generally up to 16 channels. *Dense Wavelength Division Multiplexing (DWDM)* systems have 12.5GHz to 100GHz channel spacings and generally utilize

a high number of active wavelengths. *International Telecommunication Union (ITU)* has introduced two standardizations that determine the channel spacings for CWDM and DWDM systems. ITU_T G.694.2 [1] frequency grid is for CWDM applications and supports 20 nm channel spacings between 1310nm and 1610nm. ITU_T G.694.1 [2] is for DWDM applications. It is anchored to 193.1 THz, supports a variety of channel spacings ranging from 12.5 GHz to 100 GHz and wider.

A number of multi wavelength tunable WDM sources have been demonstrated using several schemes. Among these, tunable multi-section lasers [3], external cavity diode lasers [4] and all-fiber tunable fiber lasers [4], [6] have attractive features. Tunable multi-section lasers offer small size; however their complicated fabrication steps lead to high costs. External cavity diode lasers have simpler structures but they tend to have large coupling losses due alignment problems. On the other hand, all-fiber tunable lasers provide low loss, structural simplicity and low cost.

One of the most common techniques used by tunable multi-wavelength lasers is to make use of a grid filter that is tuned to the ITU-WDM grid. At the second stage, an adjustable filter is used to select the channels provided by the grid filter. Fiber Sagnac loop filters have promising features as grid filters particularly for fiber lasers. They offer all-fiber simple structures, low insertion losses, and polarization independence.

The aim of this thesis is to build a multi-wavelength fiber source using a fiber Sagnac loop filter. The working principle of the source is similar to a resonator. Within a closed fiber loop, an EDFA is used as an amplifier and a two-stage filter system is used to produce the desired wavelength or desired set of wavelengths. The first stage of the filter is the Sagnac filter that produces a set of wavelengths. The second stage is an adjustable FBG that is used to select up to three desired channels among the wavelengths that are produced by the Sagnac filter.

The working principle of the Sagnac loop filter is closely related to polarization concept. In chapter 2 polarization, as well as the mathematical tools to analyze the

state of polarization are investigated in detail. Chapter 3 includes information about fiber lasers and other key devices used in the laser setup. Chapter 4 gives details about the experiment setup and states the results. In Chapter 5 conclusions are discussed.

CHAPTER 2

POLARIZATION AND MATHEMATICAL TOOLS TO ANALYZE STATE OF POLARIZATION

Polarization is a key concept in understanding the working principle of Sagnac loop filter. In this chapter polarization concept is presented along with the mathematical tools to analyze the state of polarization.

2.1 Polarization

Light waves are electromagnetic fields. To completely describe an electromagnetic wave four basic field vectors E, H, D, B are needed. Among these four vectors electric field vector E is chosen to define the state of polarization of the light waves. Electric field vector of a monochromatic light oscillates sinusoidal in time. If the propagation direction is taken as z direction, the electric field vector will lie in the x-y plane. The time-varying oscillation of the electric field vector can be thought of as the combination of two orthogonal components – one oscillating in x-direction and the other in y-direction. Each of these components oscillates independently at a definite frequency. The combination of these two independently oscillating components that are at right angles to each other is a vector that draws an ellipse in time. This ellipse is generally referred as the *polarization ellipse*.

If the transverse components of the electric field are represented by

$$E_x(z, t) = E_{0x} \cos(\omega t - kz + \delta_x)$$

$$E_y(z, t) = E_{0y} \cos(\omega t - kz + \delta_y)$$

where E_{0x} and E_{0y} are the maximum amplitudes and δ_x and δ_y are the phases, the equation for the polarization ellipse is

$$\frac{E_x^2}{E_{0x}^2} + \frac{E_y^2}{E_{0y}^2} - 2 \frac{E_x E_y}{E_{0x} E_{0y}} \cos \delta = \sin^2 \delta$$

where $\delta = \delta_y - \delta_x$.

For certain cases the polarization ellipse may degenerate into a line (linear polarization) or a circle (circular polarization). A complete description of the polarization ellipse must also include the sense of revolution of the electric field vector tracing the ellipse. That is, polarization is said to be left handed if the tip of the electric field vector is moving in clockwise direction when viewed by an observer facing the approaching wave, and right handed otherwise. The shape and the azimuthal orientation of the polarization ellipse that the electric field vector traces in time is called the *state of polarization (SOP)* of light.

2.2 Mathematical tools used to analyze State of Polarization

Using direct algebraic methods to solve problems involving interaction of light with elements that change the polarization of light is very tedious. Consequently various methods were developed to simplify these calculations. Stokes parameters together with Mueller matrices, Jones formalism and Poincaré sphere are the various methods to help determine the state of polarization of light in optical systems.

2.2.1 The Stokes parameters

There are various issues associated with representing the state of polarization of light using the polarization ellipse. The electric field vector traces the polarization ellipse in a time interval of the order 10^{-15} seconds. This is too short of an interval to be tracked, making the polarization ellipse impossible to observe. Furthermore, the polarization ellipse is useful only when working on completely polarized light.

However in many cases light is either unpolarized, meaning it is a mixture of plane-polarized light in all directions (e.g. sunlight or candle light), or partially polarized.

In 1852, Sir George Gabriel Stokes (1819-1903) proposed a new description for the polarization of light [7] in terms of measurable quantities, now known as the *Stokes parameters*. Stokes parameters are also applicable to unpolarized or partially polarized light, because they describe light in terms of intensity and not in terms of amplitude.

Taking the time average of the terms of the polarization ellipse equation, and rearranging we have

$$(E_{0x}^2 + E_{0y}^2)^2 = (E_{0x}^2 - E_{0y}^2)^2 + (2E_{0x}E_{0y} \cos \delta)^2 + (2E_{0x}E_{0y} \sin \delta)^2$$

The Stokes parameters are

$$S_0 = (E_{0x}^2 + E_{0y}^2)^2$$

$$S_1 = (E_{0x}^2 - E_{0y}^2)^2$$

$$S_2 = (2E_{0x}E_{0y} \cos \delta)^2$$

$$S_3 = (2E_{0x}E_{0y} \sin \delta)^2$$

The first parameter, S_0 , is the total intensity of the light. The second parameter, S_1 , indicates the amount of linear horizontal or vertical polarization. The third parameter, S_2 , indicates the amount of linear $+45^\circ$ or -45° polarization and the last parameter S_3 indicates the amount of right or left circular polarization within the beam.

These four parameters can be written as a column matrix that is called the Stokes vector

$$S = \begin{bmatrix} S_0 \\ S_1 \\ S_2 \\ S_3 \end{bmatrix}$$

The Stokes parameters for elliptically polarized light is then

$$S = \begin{bmatrix} E_{0x}^2 + E_{0y}^2 \\ E_{0x}^2 - E_{0y}^2 \\ 2E_{0x}E_{0y} \cos \delta \\ 2E_{0x}E_{0y} \sin \delta \end{bmatrix}$$

This is also called the *Stokes vector* for a plane wave. The Stokes vectors for linearly and circularly polarized light can be easily derived from this vector. Refer Appendix A to see Stokes vectors for various linearly and circularly polarized light.

2.2.2 Mueller Matrices

Consider the case where a beam of light interacts with an element that alters its SOP. Both the incident and the emerging beams can be represented by different Stokes parameters. Assuming that the parameters of the emerging beam can be written as a linear combination of the parameters of the incident beam, we have the relations

$$S_0' = m_{00}S_0 + m_{01}S_1 + m_{02}S_2 + m_{03}S_3$$

$$S_1' = m_{10}S_0 + m_{11}S_1 + m_{12}S_2 + m_{13}S_3$$

$$S_2' = m_{20}S_0 + m_{21}S_1 + m_{22}S_2 + m_{23}S_3$$

$$S_3' = m_{30}S_0 + m_{31}S_1 + m_{32}S_2 + m_{33}S_3$$

where S_0, S_1, S_2 and S_3 are the Stokes parameters for the incoming beam and S_0', S_1', S_2', S_3' are the Stokes parameters for the emerging beam.

Expressed in matrix form

$$\begin{bmatrix} S_0' \\ S_1' \\ S_2' \\ S_3' \end{bmatrix} = \begin{bmatrix} m_{00} & m_{01} & m_{02} & m_{03} \\ m_{10} & m_{11} & m_{12} & m_{13} \\ m_{20} & m_{21} & m_{22} & m_{23} \\ m_{30} & m_{31} & m_{32} & m_{33} \end{bmatrix} \begin{bmatrix} S_0 \\ S_1 \\ S_2 \\ S_3 \end{bmatrix}$$

or

$$S' = M S$$

where S and S' are the Stokes vectors and the 4x4 matrix M is called the *Mueller matrix*, named after Hans Mueller who introduced the matrix by early 1940's.

The polarization state of light can be changed by one of the following

1. Changing the amplitudes of the orthogonal basis states.
2. Changing the phase between the basis states.
3. Changing the direction of the orthogonal field components.
4. Transferring energy from polarized states to unpolarized states.

An optical element that changes the amplitude of the orthogonal basis states is called a *polarizer*. An optical element that changes the phase between the orthogonal components is called a *retarder*. If the optical component rotates the orthogonal components then it is called a *rotator*. Finally if an optical component causes energy in polarized states to go to the unpolarized states it is called a *depolarizer*. Refer Appendix B to see Mueller matrices for various components.

2.2.3 Jones Formalism

Jones formalism uses *Jones vectors* to describe the state of polarization of polarized light, and *Jones matrices* to define the polarization changing effects of optical components. It was proposed by R. C. Jones in 1941 [8].

The electric field vector of a monochromatic plane wave propagating in the +z direction can be expressed as

$$E(z, t) = \text{Re}\{E e^{j(\omega t - kz)}\}$$

E is a complex vector that lies in the x-y plane

$$E = a_x E_x e^{j\delta_x} + a_y E_y e^{j\delta_y}$$

where a_x and a_y are unit vectors and δ_x and δ_y are the phases in x and y directions respectively. Jones formalism uses this fact that the electric field vector may be represented as a linear combination of two basic polarization vectors, called the *basis states* that are orthogonal to each other and to the axis of the fiber.

Let

$$E_x(z) = E_x e^{j\delta_x}$$

$$E_y(z) = E_y e^{j\delta_y}$$

The Jones vector, expressed in terms of complex amplitudes of a plane wave is

$$J = \begin{bmatrix} E_x(z) \\ E_y(z) \end{bmatrix} = \begin{bmatrix} E_x e^{j\delta_x} \\ E_y e^{j\delta_y} \end{bmatrix}$$

Note that the elements of the Jones vector are complex numbers.

The Jones vector contains the complete amplitude and phase information and thus specifies the wave uniquely. If we are only interested in state of polarization of the wave, normalized Jones vectors may be used. A normalized Jones vector satisfies the condition

$$\bar{J}^* \cdot \bar{J} = 1$$

See Appendix A for Jones vectors of light in various states of polarization.

Jones formalism is based on the definition of the coordinate system to be used. The convention used in this thesis is as follows:

The two ends of any optical component are denoted by 1 and 2, 1 denoting the input end. The propagation direction is thus from z_1 to z_2 .



Figure 2 Convention used for Jones formalism - the propagation directions

At the input side we arbitrarily choose two directions that are orthogonal to each other and the z direction so that $\{x_1, y_1, z_1\}$ forms a right handed Cartesian coordinate system.

The electric field at the input can now be written as

$$E(z_1) = \begin{bmatrix} E_x(z_1) \\ E_y(z_1) \end{bmatrix}$$

Likewise we define a second coordinate system at the other end z_2 . $E(z_2)$ must, then, be linearly related to $E(z_1)$. In matrix formulation

$$\begin{bmatrix} E_x(z_2) \\ E_y(z_2) \end{bmatrix} = \begin{bmatrix} J_{11} & J_{12} \\ J_{21} & J_{22} \end{bmatrix} \begin{bmatrix} E_x(z_1) \\ E_y(z_1) \end{bmatrix}$$

or

$$E(z_2) = J E(z_1)$$

J is called the Jones matrix. For a chosen set of input and output coordinates, the matrix J is a characteristic attribute of the fiber component in between.

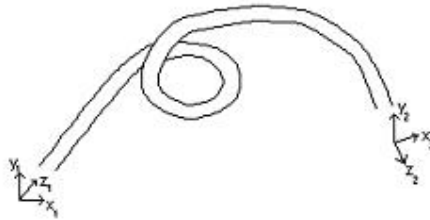


Figure 3 Convention used for Jones formalism - all input & output directions

Refer Appendix C to see Jones matrices for various polarizers and retarders and Appendix D for relationships between Mueller and Jones matrix elements.

2.2.4 Poincaré Sphere

Poincaré sphere is another method to simplify calculations regarding changes in state of polarization. It was introduced by Henri Poincaré in 1892 [9]. Poincaré discovered that the polarization ellipse could be represented on a complex plane and the complex plane could be projected onto a sphere. Therefore any SOP can be represented by a point on the sphere.

Thus, any point on the sphere corresponds to the three Stokes parameters S1, S2, and S3. Interaction of light with an optical polarizing element corresponds to a rotation of the sphere, and the new point describes the new set of Stokes parameters for the output light.

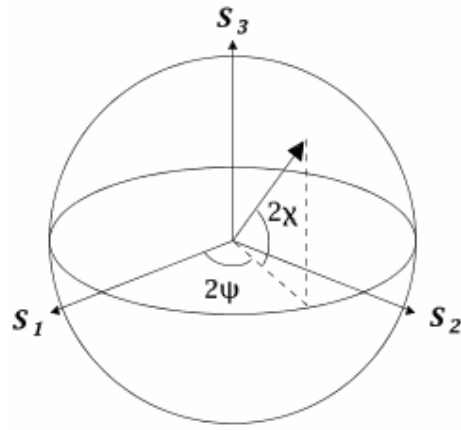


Figure 4 Poincaré Sphere

CHAPTER 3

FIBER LASERS

The term laser is short for light amplification by stimulated emission of radiation. Lasers are in fact a special form of masers (short for microwave amplification by stimulated emission of radiation). The basic principles that make up the foundation of masers were introduced by Albert Einstein in 1916. Years later, in 1953 Charles Hard Townes produced the first maser. The working principle of a maser is the same as that of a laser except a maser produces microwaves instead of optical radiation. A few years later, in 1957, Charles H. Townes together with Arthur Leonard Schawlow made the first maser that produced radiation at optical frequencies [10]. The device was then known as an optical maser. The first use of term laser was by Gordon Gould, in a paper titled "The LASER, Light Amplification by Stimulated Emission of Radiation" that was published in 1959.

The working principle of lasers depends on “population inversion” concept. To understand the concept, let’s assume that the atoms of a certain medium can be in one of the two energy states. Let N_1 denote the number of atoms in the lower energy level E_1 (called the ground level) and let N_2 denote the number of atoms in the higher energy level E_2 . And let N denote the total number of atoms $N = N_1 + N_2$

Laws of thermodynamics state that under thermal equilibrium the number of atoms in the ground level will always be much higher than the number of atoms in the higher energy level (i.e. $N_1 \gg N_2$). However the medium can be excited with energy causing the number of atoms to be in the higher energy level to increase. When the

number of atoms in the higher energy level is more than the number of atoms in the ground level, population inversion is achieved.

If photons with energy $E_{p1} = E_2 - E_1$ are released in a medium that has population inversion, some of these photons may perturb an atom of the medium that is at the higher energy level. With certain probability that depends on the number of atoms in the higher energy level, such an atom may return to the ground level, releasing a photon with energy

$$E_{p2} = E_2 - E_1 = E_{p1}.$$

This new photon has the same frequency and phase with the first photon. Furthermore the first photon is not absorbed by the atom; therefore after the collision there are two photons that are coherent. This coherent optical amplification is the basic idea behind working principle of lasers.

For a fiber laser, the medium for amplification is a rare earth doped (generally erbium) fiber. The signal and the pump power are coupled into this fiber via a special coupler, called the WDM coupler. A WDM coupler is a 2 to 1 coupler that is manufactured to combine the pump power at 980nm or 1480nm and the signal around 1550nm.

In the following sections important optical components that make up our fiber laser are investigated in detail.

3.1 Optical components that make up the fiber Laser

This section includes detailed information about various optical components that are used in the fiber laser setup. Theories that explain the working principle of component is also given.

3.1.1 Erbium Doped Fiber Amplifiers

Erbium doped fibers can be modeled with a three level laser system. In fact it can be shown that a two level system mentioned above can never achieve population inversion. Such a system can at best have population equilibrium (i.e. $N_1=N_2$). Therefore for lasing to occur a system with at least three energy levels is needed. The difference between a two level system and a three level system is that in a three level system, there is a metastable level that is between the pump level and the ground level. Atoms pumped to the pump level decay to the metastable level very quickly. The system is depicted in the Figure 5. Level 1 is the ground level, level 2 is the metastable level and level 3 is the pump level. As described in [11], the desired lasing takes place between levels 1 and 2.

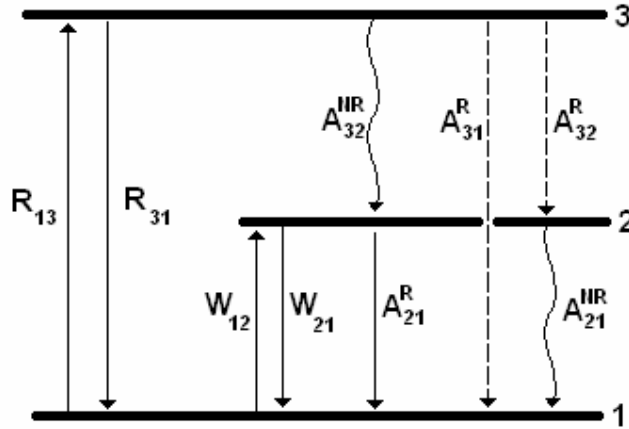


Figure 5 Three level model of EDF

R_{13} is the pumping rate and R_{31} is the stimulated emission rate from level 3 to level 1. Atoms at the pump level can have a non-radiative decay to level 2 (A_{32}^{NR}) or have radiative decays to levels 1 (A_{31}^R) and 2 (A_{32}^R). The total radiative decay from level 3 is $A_3^R = A_{31}^R + A_{32}^R$. At level 3, the non-radiative decay is dominant (i.e.

$A_{32}^{NR} \gg A_3^R$). Also it is assumed that the non-radiative decay is mostly to level 2 (i.e. $A_{32}^R \gg A_{31}^R$). Thus we can safely assume that A_{32}^R constitutes the main spontaneous decay from level 3 (A_{32}). W_{12} and W_{21} are stimulated absorption and emission rates respectively between levels 1 and 2. $A_{21}^R = 1/\tau$ is the radiative decay from level 2 to level 1, where by definition τ is the fluorescence lifetime. A_{21}^{NR} is the non-radiative decay from level 2 to level 1. The total spontaneous decay from level 2 is $A_{21} = A_{21}^R + A_{21}^{NR}$. At level 2 spontaneous decay is mostly radiative (i.e. $A_{21}^R \gg A_{21}^{NR}$). Let N_1 , N_2 and N_3 denote the fractional populations of atoms in energy levels 1, 2 and 3 respectively and let ρ denote the total laser ion density (i.e. $\rho = N_1 + N_2 + N_3$)

The atomic rate equations corresponding to these populations is then

$$\frac{dN_1}{dt} = -R_{13}N_1 + R_{31}N_3 + W_{12}N_1 + W_{21}N_2 + A_{21}N_2$$

$$\frac{dN_2}{dt} = W_{12}N_1 - W_{21}N_2 - A_{21}N_2 + A_{32}N_3$$

$$\frac{dN_3}{dt} = R_{13}N_1 - R_{31}N_3 - A_{32}N_3$$

At steady state where populations do not change $dN_i/dt = 0$ ($i=1, 2, 3$). To simplify the equations let's define

$$a = R_{31} + A_{32} \text{ and } b = W_{21} + A_{21}$$

then

$$W_{12}N_1 - bN_2 + A_{32}N_3 = 0$$

$$R_{13}N_1 - aN_3 = 0$$

replacing $N_3 = \rho - N_1 - N_2$ and solving for N_1 and N_2

$$N_1 = \rho \frac{ab}{b(a + R_{13}) + aW_{12} + R_{13}A_{32}}$$

$$N_2 = \rho \frac{R_{13}A_{32} + aW_{12}}{b(a + R_{13}) + aW_{12} + R_{13}A_{32}}$$

Replacing $a = R_{31} + A_{32}$, $b = W_{21} + A_{21}$ and factorizing the term $A_{21}A_{32}$,

$$N_1 = \rho \frac{(1 + W_{21}\tau) \left(1 + \frac{R_{13}}{A_{32}}\right)}{(1 + W_{21}\tau) \left(1 + \frac{R_{13} + R_{31}}{A_{32}}\right) + W_{12}\tau \left(1 + \frac{R_{31}}{A_{32}}\right) + R_{13}\tau}$$

$$N_2 = \rho \frac{R_{13}\tau + W_{12}\tau \left(1 + \frac{R_{13}}{A_{32}}\right)}{(1 + W_{21}\tau) \left(1 + \frac{R_{13} + R_{31}}{A_{32}}\right) + W_{12}\tau \left(1 + \frac{R_{31}}{A_{32}}\right) + R_{13}\tau}$$

Further assume that the nonradiative decay rate A_{32} is much higher than the pumping rate and stimulated emission rate for the pump level (i.e. $A_{32} \gg R_{13,31}$), and let $R=R_{13}$, then

$$N_1 = \rho \frac{1 + W_{21}\tau}{1 + R\tau + W_{12}\tau + W_{21}\tau}$$

$$N_2 = \rho \frac{R\tau + W_{21}\tau}{1 + R\tau + W_{12}\tau + W_{21}\tau}$$

Since nonradiative decay A_{32} is dominant, the population at pump level is negligible:

$$N_3 = \rho - N_1 - N_2 = 0$$

The steady state populations are one of the main determining factors for the gain coefficient in erbium doped fibers. When a light beam with intensity I_s traverses a certain length of erbium doped fiber the change of intensity is given by [12], [13].

$$\frac{dI_s}{dz} = \{\alpha_e(\lambda_s)N_2 - \alpha_a(\lambda_s)N_1\}I_s$$

where $\alpha_a(\lambda_s)$ and $\alpha_e(\lambda_s)$ are the absorption and emission cross sections of the laser transition at the wavelength λ_s .

Pumping of an EDF may be done using various combinations. The basic forward pumping scheme is shown in Figure 6. Using a backward pumping scheme is also possible as depicted in Figure 7

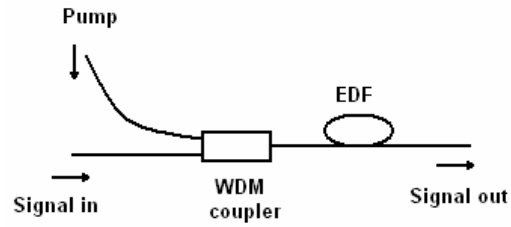


Figure 6 The basic forward pumping scheme for EDFA

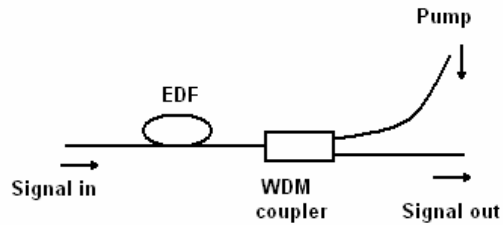


Figure 7 Backward pumping for an EDFA

In telecommunication links using the same fiber for bidirectional signaling may be cost effective. In such cases bidirectional pumping is used. The simplest bidirectional pumping is shown in Figure 8. Although simple, this setup may have serious BER penalties due to backreflections since no optical isolators are used.

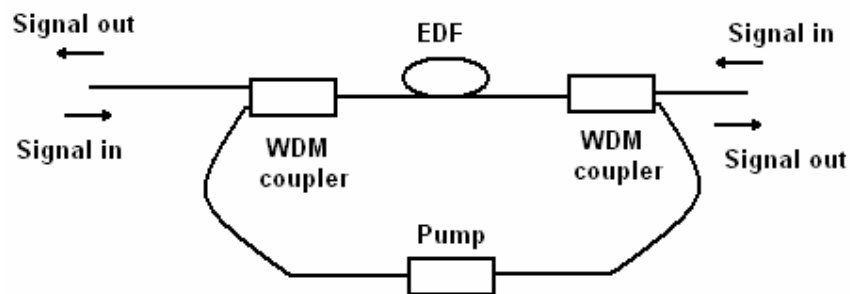


Figure 8 Bi-directional pumping for EDFA

3.1.2 Birefringence Concept and Polarization Maintaining Fibers

Birefringence phenomenon was first seen in crystals. In some crystals like calcite, ruby, sapphire molecular structure causes the material to behave like it has two different refractive indices in different directions. Thus these materials are said to have bi-refrignence. Hexagonal, tetragonal, and trigonal crystal classes exhibit birefringence. Orthorhombic, monoclinic, triclinic crystal classes like borax, topaz, ulexite, exhibit three indices of refraction. They are therefore trirefringent.

Theoretically when linearly polarized light is launched into a fiber that has perfect circular symmetry, if the fiber has no bending (i.e. it is laid straight) the input light will maintain its polarization state throughout the fiber. However in practice, fibers cannot be manufactured with perfect cylindrical shapes. There are radius variations along the fiber. These intrinsic imperfections, together with external influences like

fiber bends, stresses, vibrations, changes in temperature, etc. lead to random regional birefringence effects along the fiber. This random birefringence causes different propagation constants of the basis modes which causes random coupling between the two modes. This, in turn, causes the polarization to randomly vary along the length of the fiber.

One way to reduce the amount of coupling between the modes is to introduce strong linear or circular birefringence into the fiber. This is the idea behind polarization maintaining fibers. They can be classified into two major groups. High birefringence fibers, which try to combat the random birefringence effect by introducing even stronger linear birefringence along the fiber and low birefringence fibers, which try to eliminate the random birefringence effects by introducing circular birefringence.

The main principle of high-birefringence polarization maintaining fibers is that, the effect of the intentionally introduced linear birefringence will dominate the random birefringence and the effect of azimuthal imperfections and external influences will now be negligible. This intentionally introduced birefringence, also called the modal birefringence, is expressed as

$$B_F = \frac{(\beta_x - \beta_y)}{2\pi/\lambda}$$

where β_x and β_y are the propagation constants of the basis modes and λ is the optical wavelength.

If linearly polarized light along one of the principle axis is launched into a high birefringence polarization maintaining fiber, due to the intentionally introduced strong birefringence, no coupling to the other basis state will occur, thus light will retain its polarization state throughout the fiber and the polarization will be maintained.

A measure the strength of birefringence in a PM fiber is the beat length. When linearly polarized light that is 45° to the principle axis is launched into a hi-bi fiber,

it has two components that have equal power each traveling along one of the principle axis. The component along the axis with the higher refractive index (called the slow axis) travels slower than the component along the axis with the lower refractive index (called the fast axis). This introduces a linear retardation $\Phi(z)$ between the components which depend on the fiber length.

$$\Phi(z) = (\beta_x - \beta_y)L$$

It is this retardation that stops power coupling between the principle modes.

Since one component is lagging behind the other, light will periodically change its state of polarization through a series of elliptical, circular, and linear states. The length of fiber that the polarization of light undergoes a complete cycle of these states is called the *beat length*. This situation is shown in Figure 9.

The polarization becomes circular at $\Phi=\pi/2$ and linear again at $\Phi=\pi$, circular once more at $\Phi=3\pi/2$ and finally returns to its original SOP at $\Phi=2\pi$. The most commonly used method to measure beat length a helium-neon laser operating at 633nm is launched into the fiber at 45 degrees to the birefringent axes so that equal optical power is coupled into both axes. Rayleigh scattering within the fiber causes alternating regions of light and dark to appear. The dark regions appear each time the polarization state within the fiber returns to linear, in the direction of observation. Beat length is a measure of how strongly birefringent the fiber is. It is one of the main parameters that define the characteristics of a PM fiber.

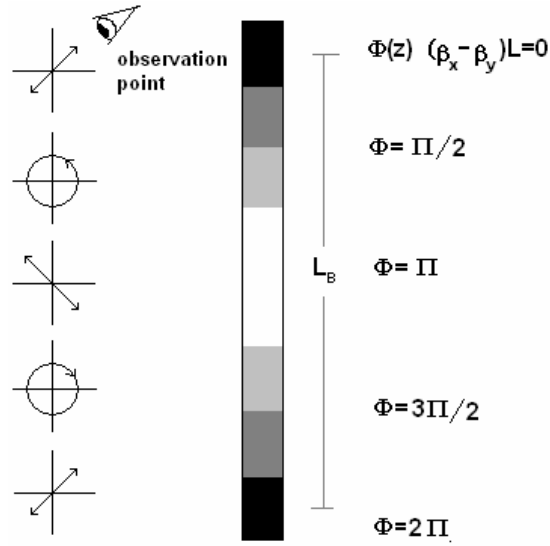


Figure 9 An illustration of beat length

Both the high birefringence and the low birefringence fibers can be further categorized. High birefringence fibers have two types called the single polarization fibers and two-polarization fibers. Single polarization fibers impose a cutoff condition on one of the modes to allow only one polarization mode.

Another criterion for the classification of polarization maintaining fibers is the way the stress is applied. There are mainly two types. Birefringence introduced via geometrical effect and birefringence introduced via stress effect. Geometrical birefringence is a weaker effect. These fibers are constructed with a large refractive index difference between the core and the cladding to obtain high birefringence. This is accomplished by using higher doping levels, which leads to increased optical losses [14].

Stress birefringence may be introduced by placing asymmetrical stress inducing elements along the fiber as in PANDA (polarization maintaining and absorption reducing) or bow-tie type hi-bi PM fibers or making the fiber core non-circular as in elliptical core type hi-bi PM fibers.

The idea behind low birefringence fibers is to fabricate near-perfect round shaped core fibers and introduce circular birefringence for example by spinning the fiber. Introducing high circular birefringence causes two orthogonally polarized modes to be clockwise and counterclockwise circular polarized, causing these two circular polarized modes to be decoupled. Increased the circular birefringence causes an effect of averaging out the linear birefringence. That's why these fibers are called low birefringence polarization maintaining fibers.

One type of low birefringence fibers is the round core fibers. Round core fibers may have an ellipticity of less than 0.1% [15], [16]. To introduce circular birefringence fiber may be twisted. It is shown that a twist rate of around five turns per meter is sufficient to significantly reduce coupling between the polarization modes [17]. However this method has limitations. Twisted fiber is more fragile thus it is harder to handle. Also it is hard to obtain beat lengths lower then 10 cm with this method because fiber tends to break at high twist rates.

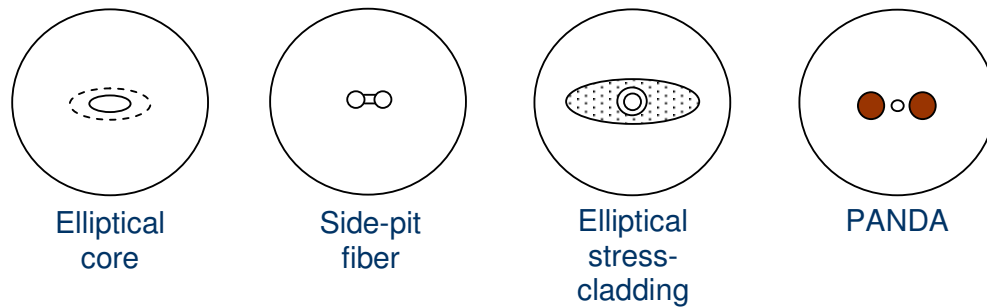


Figure 10 Structures of various polarization maintaining fibers

To obtain lower beat lengths without damaging the fiber, the glass preform can be rotated during the fiber drawing process. Such fibers are called *spun* fibers. This method also decreases the linear birefringence by introducing circular birefringence, also, since the fiber is spun while in perform state, there is no shear stress. This technique has been used to produce fibers with birefringence as low as 4.3×10^{-9} [17].

Circular birefringence can also be introduced by making the core of a fiber follow a helical path inside the cladding as in Figure 11. This makes the propagating light, constrained to move along a helical path, experience an optical rotation [18], [19].

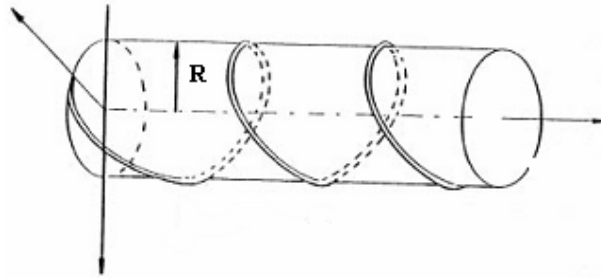


Figure 11 Structure of a helical core fiber

PM Fibers	High Birefringence	Single Polarizing	Geometrical	Side-pit
			Effect	Side-tunnel
			Stress Effect	Bow-tie
				Flat cladding
				PANDA
				Stress guiding
		Two Polarizing	Geometrical Effect	Elliptical core
				Dumbbell core
				Four section core
				Side-pit
				Side-tunnel
			Stress Effect	Elliptical cladding
				Elliptical jacket
				Bow-tie
				Flat cladding
				PANDA
	Low Birefringence	Geometrical Effect	Round core	
			Spun	
		Stress Effect	Twist	

Figure 12 Types of PM fibers

3.1.3 Fiber Bragg Gratings

A Fiber Bragg Grating is a passive optical component, which is mainly used as a reflection filter. The reflection is caused by the periodic refractive index changes (called gratings) formed along the core of the fiber. The formation of permanent gratings in an optical fiber was first shown by Kenneth O. Hill in 1978. The gratings can be “written” on the fiber by using the *photosensitivity* of the fiber. The refractive index of the optical fiber can be changed permanently by exposing it to light at a certain wavelength such as ultraviolet light at 244nm. This is called the photosensitivity effect. Photosensitivity of the fiber was also first observed at the same experiment. A 488 nm light was launched into a single mode fiber and the reflected light was monitored. The amount of light was at first very low, however after a few minutes nearly all of the coupled light was reflected back.

The phenomenon was explained as follows: The coherent light was forming a standing wave by interacting with the light that was reflected from the end of the fiber. This standing wave was forming a grid on the fiber through photosensitivity. The formation of the grid increased the intensity of the reflected wave, which in turn increased the strength of the grid leading to a total reflection after a few minutes.

The magnitude of the refractive index change due to photosensitivity depends on a few factors such as the wavelength and the intensity of the irradiating light and the composition of the material forming the fiber core.

The periodic index variation in the core causes the energy of the fundamental mode to couple to various guided and lossy modes. The strongest mode coupling occurs at the Bragg wavelength [20].

$$\lambda_{bragg} = 2n_{eff} \Lambda$$

Here n_{eff} is the modal index and Λ is the grating period. At the Bragg Wavelength each reflection from a single crest in the index perturbation is in phase with each other.

Any change in fiber properties, such as strain or temperature, will change the Bragg Wavelength. The shift in Bragg Wavelength due to strain and temperature can be expressed as [20].

$$\Delta\lambda_{bragg} = 2n_{eff} \Lambda \{1 - p_e\} \epsilon + \left[\alpha + \frac{1}{n} \left(\frac{dn}{dT} \right) \right] \Delta T$$

where ϵ is the applied stress, ΔT is the temperature change and α is the thermal expansion coefficient. Finally p_e is a term that includes the effects of photo elastic contributions and can be defined as

$$p_e = \left(\frac{n^2}{2} \right) [P_{12} - \mu(P_{11} + P_{12})]$$

in terms of fiber Pockel's coefficients P_{ij} and the Poisson ratio μ .

The important issue to note here is that the change in Bragg Wavelength is proportional to both strain effects (ϵ) and temperature changes (ΔT). We will use this property to obtain an adjustable wavelength filter in our setup.

3.1.4 Fiber Couplers

When two waveguides are placed very close to each other as shown in Figure 13, light “couples” from one waveguide to the other. If the core regions of two fibers are brought together by stripping their claddings, the evanescent field of the first fiber penetrates into the core region of the other fiber. The amount of coupled energy increases with the *coupling length*. After a certain amount of length, light in the first fiber couples to the second fiber completely. Then it starts to couple back to the first fiber. This coupling continues back and forth periodically. *Mode coupling theory* can be utilized to better understand the phenomenon.

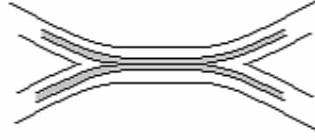


Figure 13 A fiber coupler formed by bringing the core regions close

The electric field of the propagating mode in the waveguide is described by

$$E(x, y, z) = A(z)\mathcal{E}(x, y)$$

where $A(z)$ is a complex amplitude which includes the phase term $\exp(-j\beta z)$ and $\mathcal{E}(x, y)$ is the solution for the field distribution of the mode in one waveguide, assuming the other waveguide is absent. By convention $\mathcal{E}(x, y)$ is assumed to be normalized to carry one unit of power. Thus, for example, the power in guide number 1 is given by

$$P_1(z) = |A_1(z)|^2 = A_1(z) \cdot A_1^*(z)$$

The coupling between modes is given by the general coupled mode equations for the amplitudes of the two modes. Thus,

$$\frac{dA_0(z)}{dz} = -j\beta_0 A_0(z) + \kappa_{01} A_1(z)$$

and

$$\frac{dA_1(z)}{dz} = -j\beta_1 A_1(z) + \kappa_{10} A_0(z)$$

where β_0 and β_1 are the propagating constants of the modes in the two guides.

κ_{10} and κ_{01} are the coupling coefficients between the modes. If the two waveguides are identical then $\kappa_{10} = \kappa_{01} = \kappa$.

If it is assumed that the waveguides both have an exponential optical loss coefficient α

$$\beta = \beta_r - j\frac{\alpha}{2}$$

where $\beta = \beta_0 = \beta_1$, and β_r is the real part of β .

Furthermore, if it is assumed that the light is coupled into the first waveguide at the point $z = 0$, the boundary conditions are:

$$A_0(0) = 1 \text{ and } A_1(0) = 0$$

Then the solutions can be expressed as

$$A_0(z) = \cos(\kappa z) e^{-j\beta z}$$

and

$$A_1(z) = -j \sin(\kappa z) e^{-j\beta z}$$

Thus the power flow in the guides is given by

$$P_0(z) = A_0(z) \cdot A_0^*(z) = \cos^2(\kappa z) e^{-\alpha z}$$

and

$$P_1(z) = A_1(z) \cdot A_1^*(z) = \sin^2(\kappa z) e^{-\alpha z}$$

It can be seen from these equations that the power does indeed transfer from one waveguide to the other and back as a function of the coupling length. Note also that there is a phase difference between the amplitudes of the wave in two waveguides. The phase in the driven guide always lags 90° behind the phase of the driving guide. The lagging phase relationship continues along z such that at a certain distance $\kappa z = \pi/2$ all of the power has been transferred to the second guide.

To obtain a 3dB (50/50) coupler, the coupling length must be

$$L = (2m + 1) \frac{\pi}{4\kappa} \quad m=0,1,2,\dots$$

The coupling equations can also be expressed in Jones formalism

$$\begin{bmatrix} E_{o0}(f) \\ E_{o1}(f) \end{bmatrix} = e^{-j\beta z} \begin{bmatrix} \cos(\kappa z) & j \sin(\kappa z) \\ j \sin(\kappa z) & \cos(\kappa z) \end{bmatrix} \begin{bmatrix} E_{i0}(f) \\ E_{i1}(f) \end{bmatrix}$$

where E_{i0} and E_{i1} are the input and E_{o0} and E_{o1} are the output electric fields of the first and second ports respectively.

When used with only one active input, say input 0 the power transfer function may be obtained by setting $E_{i1} = 0$:

$$\begin{bmatrix} T_{11}(f) \\ T_{12}(f) \end{bmatrix} = \begin{bmatrix} \cos^2(\kappa z) \\ \sin^2(\kappa z) \end{bmatrix}$$

$$\text{where } T_{kl}(f) = \frac{|E_{ol}|^2}{|E_{ik}|^2}$$

3.1.5 Optical Isolators and Circulators

An optical isolator is a passive device that allows light to be transmitted in one direction and blocks the light coming from the other direction. Connectors and other components, even fusion spliced fibers, cause backreflections. These backreflections cause degradation in the stability of the oscillation within the laser source causing reduced performance.

The input beam is divided into two beams polarized in basis coordinates by the use of a polarization beam splitter, then each beam goes through a polarizer, a vertical polarizer for one of the beams and a horizontal polarizer for the other. The polarization of the beams are then rotated 45 by faraday rotators. The beams pass through the output polarizers that are positioned 45 to their respective input polarizer. They are combined by a polarization beam combiner, and leave the isolator.

The light traveling backwards through the isolator is split into two by the polarization beam combiner, now working as a polarization beam splitter when the beam is input from the other end. The beams become 45° polarized to horizontal for one beam and 45° polarized to vertical for the other. They are rotated a further 45° by the Faraday rotators and are blocked by the input polarizers which are 90° to the beams polarization.

Important properties of an optical isolator are the isolation that is a measure of how effectively backreflections are suppressed, center wavelength which the device is optimized to work, bandwidth, insertion loss and polarization dependent loss. Optical circulators are similar to optical isolators. They protect the input from the reflected power. The difference of optical circulators is that they enable the use of the backreflected power through a third port. So in effect an optical circulator is a signal router that routes the power from port 1 to port 2 and the power coming into port 2 to port 3. Optical isolators are used with band-rejection type filters like FBGs to form bandpass filters. They are also used in conjunction with dispersion compensation modules to reduce dispersion.

3.1.6 Sagnac Loop Filter

Figure 14 shows the structure of the Sagnac filter. The coupler is a 3dB coupler that divides the incoming wave into two counter-propagating waves that have equal power.

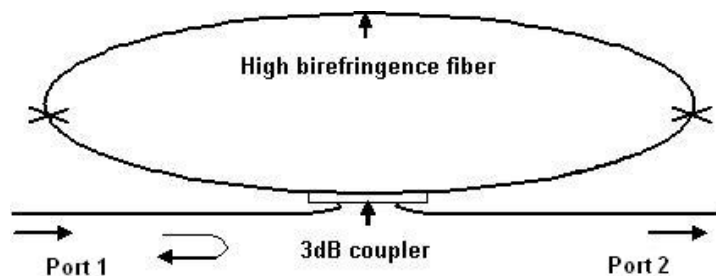


Figure 14 Structure of the fiber Sagnac loop filter

Birefringence is a lossless reciprocal phenomenon. However its effect on the state of polarization is in general nonreciprocal. The state of polarization will be different for two counterpropagating waves passing through a birefringent fiber if this birefringence is complex. We can denote the Jones matrix of the hi-bi fiber along the clockwise direction in the Sagnac loop as [21].

$$M_{cw} = \begin{bmatrix} A & -B^* \\ B & A^* \end{bmatrix}$$

The Jones matrix for the counterclockwise direction is then

$$M_{ccw} = \begin{bmatrix} A & -B \\ B^* & A^* \end{bmatrix}$$

where B is the cross coupling term and A is chosen to make $|M|=1$ since this is a lossless reciprocal system. If we denote the state of polarization at the input as

$$E_{in} = \begin{bmatrix} E_x \\ E_y \end{bmatrix}$$

the output field at port 2 will be

$$E_{out} = j \cdot \text{Im}(B) \begin{bmatrix} E_y \\ E_x \end{bmatrix}$$

due to the reciprocity of the Jones matrix [22].

According to Jones matrix theory, any birefringence effect can be represented by a combination of a linear and a circular birefringence. If we represent the linear birefringence with δ and circular birefringence with α and the reference system is selected along the principal axes of the linear birefringence, the output intensities from ports 1 and 2 will be [21]

$$I_1 = |E_1|^2 = I_{in} \sin^2(\delta/2) \sin^2(\alpha/2)$$

$$I_2 = |E_2|^2 = I_{in} \cos^2(\delta/2) + \cos^2(\delta/2) \sin^2(\alpha/2)$$

The equivalent circular birefringence α can be arranged to be $2\pi \pm \pi$ by twisting or spinning the principal axes of the linear birefringence. Then the output intensities can be expressed in simpler forms as

$$I_1 = I_{in} \sin^2(\delta/2) \text{ and } I_2 = I_{in} \cos^2(\delta/2)$$

From these equations it is clear that the output intensity of the light will change periodically with the linear birefringence. Since linear birefringence is wavelength dependent, output intensities will also be wavelength dependent. The phase difference ϕ between the fast and slow axes over a length of L is [5]

$$\phi = (2\pi / \lambda)BL$$

B is the fiber birefringence

$$B = |n_{fast} - n_{slow}| = \lambda_0 / L_B$$

where L_B is the beat length measured at λ_0 .

Since ϕ is wavelength dependent, the interference pattern produced by the counterpropagating fields consists of a period of peaks at the wavelengths where $\phi=2k\pi$ (i.e. the interference is constructive). The output has the lowest values at wavelengths where $\phi=(2k+1)\pi$ (i.e. the interference is destructive). The filter spacings are given by

$$\Delta\lambda = \lambda^2 / BL \text{ or } \Delta f = c / BL$$

The phase difference also depends temperature. This dependence has two components. One due to changes in fiber length and the other due to changes in birefringence. Changes in fiber length are three orders of magnitude smaller than the changes due to birefringence changes (i.e. $\frac{\partial\phi}{\partial T} > (2\pi / \lambda)L \frac{\partial B}{\partial T}$) [21].

CHAPTER 4

EXPERIMENTAL SETUP

In this section various tools used to obtain measurements on the source as well as the setup of the source itself are discussed in detail.

The setup we used as the optical spectrum analyzer contains an adjustable narrow width optical filter, an optical multimeter and an oscilloscope. In all the graphs obtained using this OSA setup, the second channel shows the analog input to the filter used to obtain that spectrum. A +5V on the second channel corresponds to 1560nm on the first channel, a -5 corresponds to 1520nm, with each 1V change corresponding to a 4nm change. Therefore, for example to determine the wavelength of a certain peak, one should mark its place on the x-axis, note the voltage value of the signal at the second channel for the same x-axis value, and calculate the corresponding wavelength.

The intensity values may be determined by utilizing two facts:

- A 3dB change halves the voltage
- An intensity 10dBm more than the set scale corresponds to 1.5 volts.

Therefore when the multimeter is set to -40dBm scale, 1.5V on the oscilloscope corresponds to -30dBm and 0.75V corresponds to -33dBm, etc.

Details about the OSA setup can be found in appendix E

4.1 The Structure of the Source

The structure of the source is depicted in Figure 15 and a photo of the setup is shown in Figure 16. There are three main components that make up the source. These are EDFA, the Sagnac loop filter and the adjustable filter.

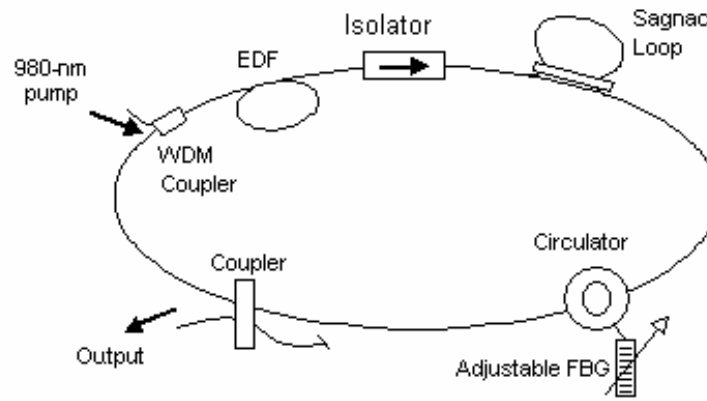


Figure 15 Structure of the laser

Wideband light is obtained at the output of the pumped EDF. The Sagnac loop filter produces a grid output when its input is wideband light. The adjustable filter setup chooses the desired wavelength. An optical isolator is used to suppress the counterpropagating wave from the Sagnac loop as well as any backreflections. The output is obtained via a 50/50 coupler.

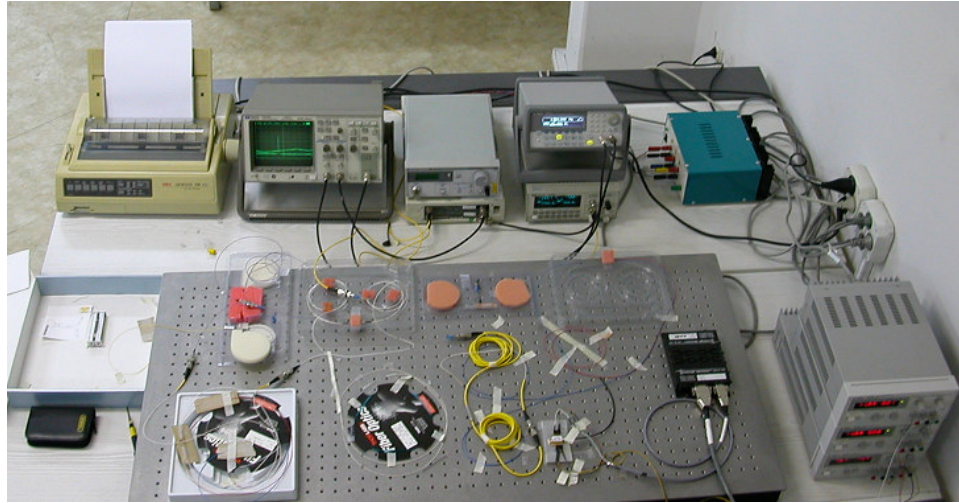


Figure 16 A photograph of the setup

Sagnac filter consists of a 50/50 coupler fusion spliced to a hi-bi PM fiber. We tested two kinds of hi-bi fibers for the Sagnac filter. One of them is a 10m long doubly clad elliptic core fiber and the other is a 10m long PANDA fiber. Their beat lengths are 3mm and 3.6mm respectively. Insertion losses of the couplers are; 3.22/3.19dB for the coupler used in the Sagnac loop with the doubly clad PM and 3.39dB/3.31dB for the other coupler. Both couplers have a directivity of 60dB, a return loss of 55dB, polarization dependent loss smaller than 0.1dB and thermal stability smaller than 0.3 dB. Figure 17 and Figure 18 show two the comb filter outputs with these two different hi-bi fibers when a broadband source is used as an input to the loops. The average channel spacing is 0.47nm for the doubly clad fiber and 0.57nm for the PANDA fiber. The source is operated at 8mW. peak to valley ratios up to 9dBm for the PANDA fiber and up to 8dBm for the doubly clad fiber are obtained.

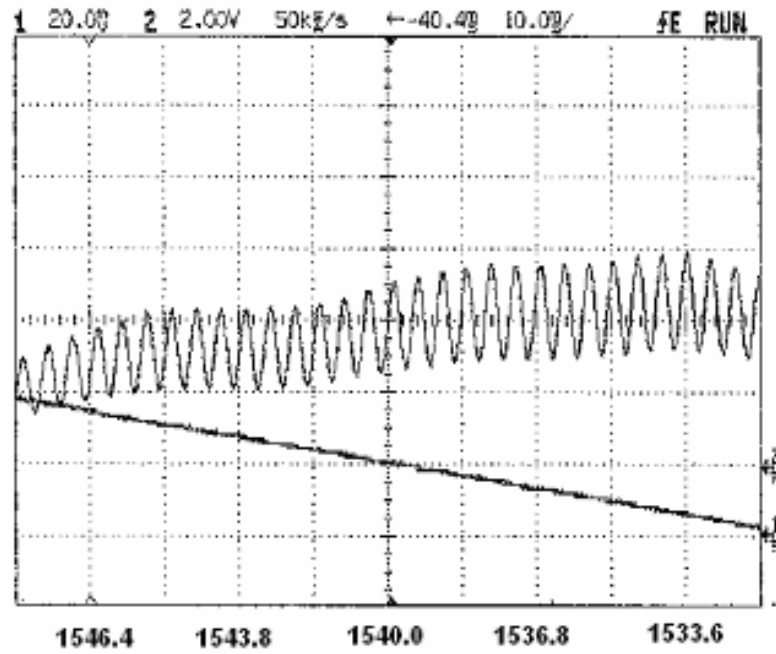


Figure 17 Frequency spectrum of the comb filter with doubly clad PM

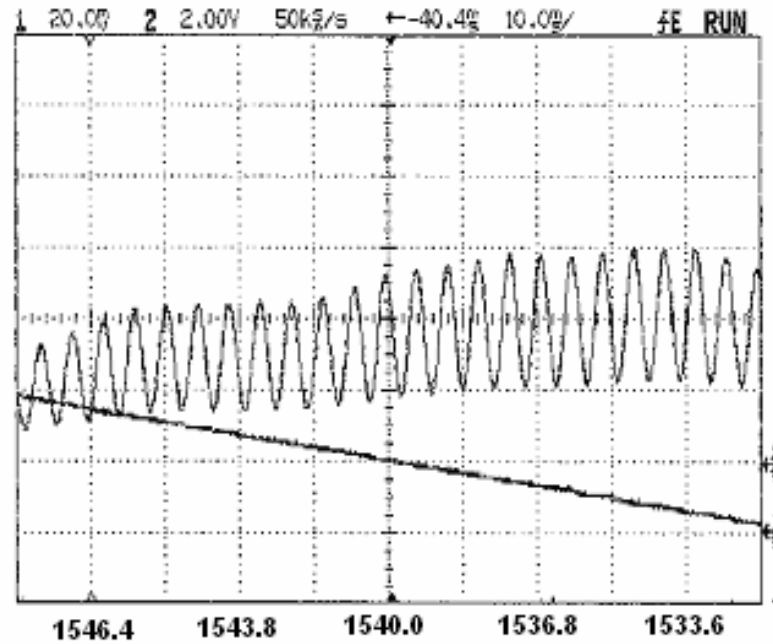


Figure 18 Frequency spectrum of the comb filter with the PANDA fiber

A pump laser operating at 980nm, a laser diode driver, 10 meters of erbium doped fiber and a WDM coupler are used in the EDFA. The laser diode driver has an output current range of 0-1A with a short term (1hr) stability that is smaller than 20ppm and a long term (24 hrs) stability that is smaller than 50ppm. The noise and ripple are smaller than 10 μ A and the current limit accuracy is 50mA. The pump laser has a maximum operating power of 135mW and a maximum operating current of 300mA. The WDM coupler has 980nm and 1550 nm central wavelengths on pump and signal paths respectively with 0.21dB and 0.16dB insertion losses. Isolation of the WDM is 24.79dB. It has a bandwidth of 10nm and a directivity of 62.83dB. The output power versus pump power is depicted in Figure 19. As seen from the graph, the output power tends to saturate as the pump power goes above a certain range. The gain spectrum of the EDFA used in the setup for a 140mA pump current is depicted in Figure 20

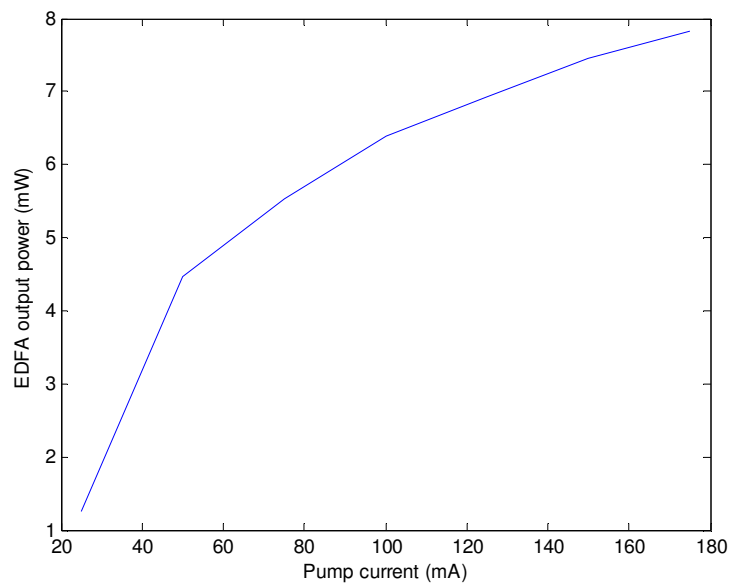


Figure 19 Output power of the EDFA vs pump current

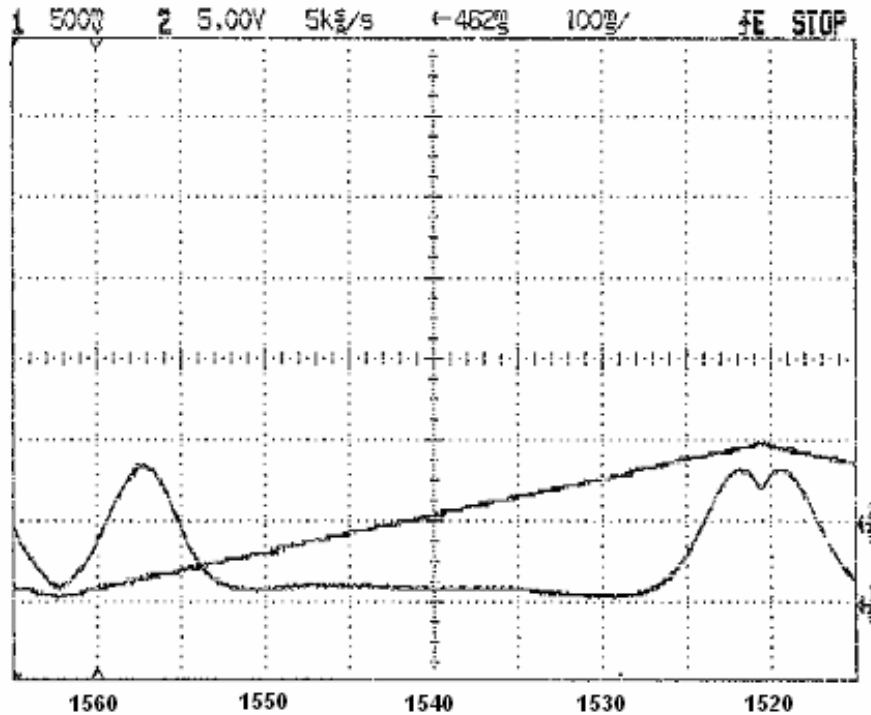


Figure 20 The spectrum of EDFA without any input

One important point to note is that the gain spectrum of the EDFA is not flat. There are peaks at around 1532nm and 1558nm with about -6dBm peak values. Before we formed our loop making up the overall laser, one of the first things we wanted to do was to see the Sagnac loop filter output within the closed feedback loop to determine how much it would get amplified. To our surprise the output of a closed loop consisting of the EDFA and the Sagnac loop filter wasn't a wavelength comb. Instead what we observed was a single peak at about 1557nm. The peak had a much larger peak to valley ratio when compared with the Sagnac loop filter's comb output peaks. This unexpected pattern wasn't stable. The single peak would move slightly to the left or right and occasionally it would split into two, sometimes three peaks. However all of these peaks were always around 1557 nm. This mysterious single peak is depicted in Figure 21.

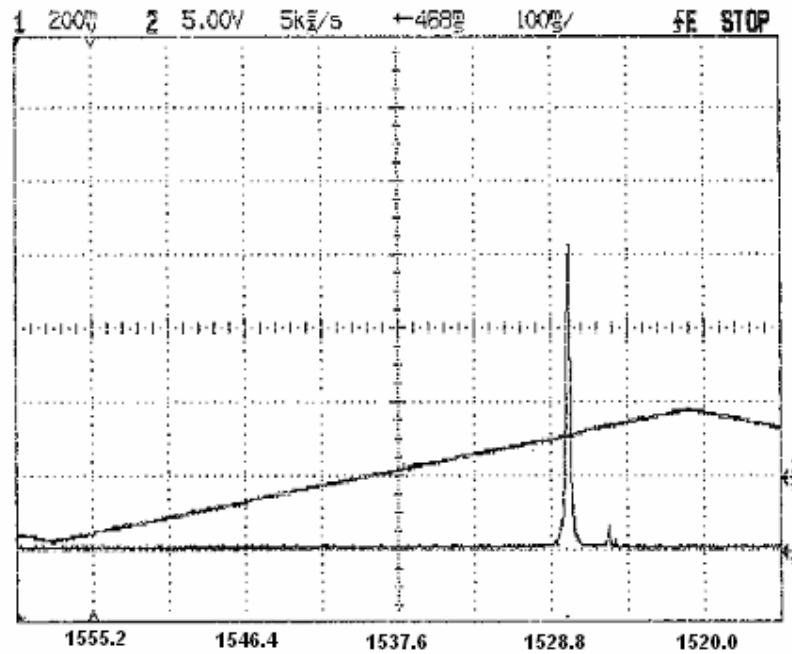


Figure 21 The self-filtering effect of the closed loop EDFA setup

Further investigation showed that this phenomenon is not related to the Sagnac loop filter at all. When an EDFA is used within a loop, the so called “self-filtering effect” occurs. As the wide-band light passes through the EDFA, the component with the wavelength for which the amplitude of the gain spectrum is largest, gets amplified more than the other wavelength components. When used in a closed feedback loop this difference becomes larger at each pass. This causes most of the power to be “confined” to that particular wavelength. Since the overall power is limited, the power at other wavelengths is suppressed, leading to a single line at the output. This is known as the *self-filtering effect*. There are various methods to flatten the gain spectrum of an EDFA to avoid the self-filtering effect; however this is not necessary for our setup since we use a two stage filtering system. The FBGs at the second stage will filter out the self-filtering wavelength.

The adjustable filter consists of a circulator, and an adjustable FBG configuration. The working principle of the FBG-circulator bandpass filter is as follows:

When a broadband light is coupled into port 1, the circulator will transfer it to port 2. If a FBG is connected to port 2, this broadband light will pass through the FBG. Since an FBG reflects a certain wavelength, this reflected light will return to the port 2 of the circulator as an input light. Circulator will transfer this light to port 3. If the other end of the FBG is connected to an APC connector no other backreflections will occur. Thus this combination can be used to filter light at a certain wavelength. The circulator we used had insertion losses of 0.7dB from port 1 to port 2 and 0.63dB from port 2 to port 3, isolations of 53 dB from port 2 to port 1 and 50dB from port 3 to port 2. Directivities are 58dB from port 1 to port2 and 68dB from port 2 to port 3. Return losses are 53 dB for port 1, 53 dB for port 2 and 54 dB for port3. Polarization dependent losses are 0.05 dB from port 1 to port 2 and 0.15dB from port 2 to port 3.

The adjustable FBG configuration is as follows Three FBGs with different central wavelengths are fusion spliced in series. Then, they are fixed by their end points onto a thin metal plate as shown in Figure 22.

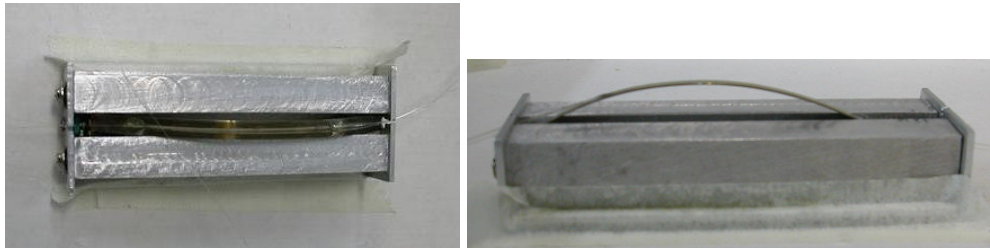


Figure 22 The adjustable FBG setup

There is a screw on one end. As this screw is rotated it pushes the metal plate, causing it to bend. Each turn of the screw pushes the metal plate 0.5mm. Figure 23 depicts the bent metal sheet and the fiber laid on it. The thickness of the metal sheet

was measured to be 0.328 mm. The radius of the fiber is 0.125mm. It is assumed that the length of the sheet at the center of its thickness does not change after bending, while its lower layer gets contracted and its upper layer gets stretched. The metal sheet has a certain bent shape even before any stretching is applied to it. Let's call the length of the sheet before it was further bent A . After the bending it can be expressed as $2\pi R(\theta/2\pi) = R\theta$. However since the bending doesn't change the length of the metal sheet $A=R\theta$. This was also the length of the fiber when it was laid on the unbent metal sheet. However after the bending the length of the fiber along its core is $\theta(R+x)$, where $x=(a/2 + t/2)$. The fiber was stretched an amount equal to $\Delta f_L = \theta(R+x) - \theta R = \theta x$.

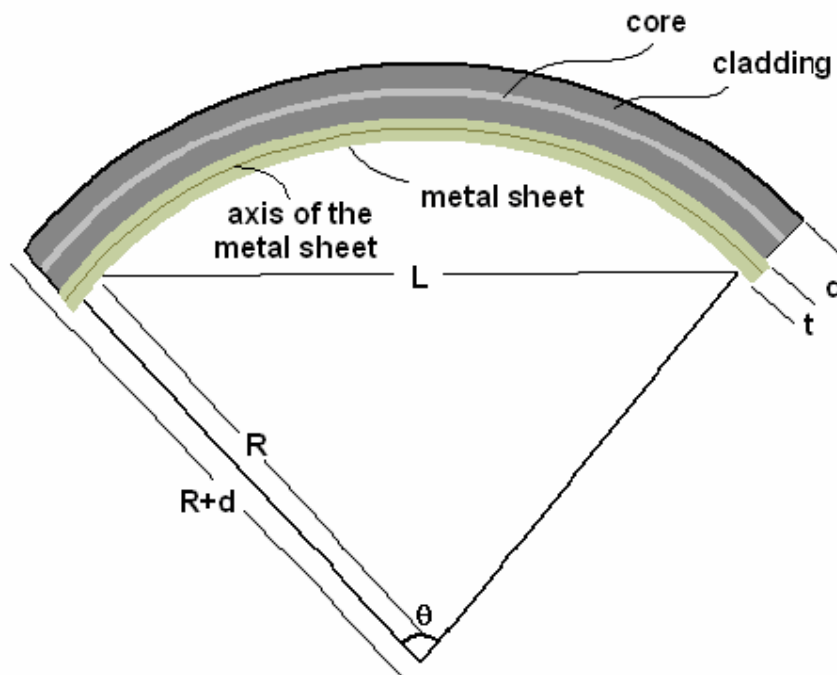


Figure 23 Bent metal sheet and the fiber laid on it

When the metal sheet is in its rest state we have a radius R_1 , an angle θ_1 and chord length L_1 . After the screw is turned a few times we have a radius R_2 , an angle θ_2 and chord length L_2 . We have $A = R_1\theta_1 = R_2\theta_2$. This is depicted in Figure 24.

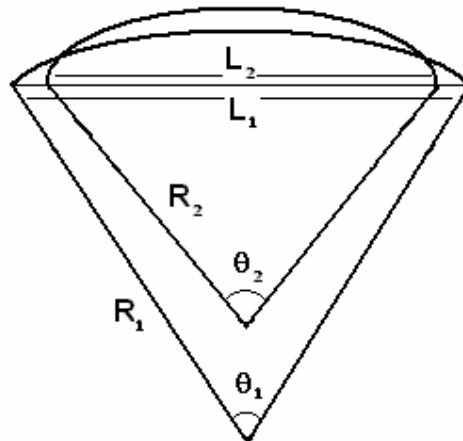


Figure 24 The metal sheet before and after applying stress

Now consider Figure 25.

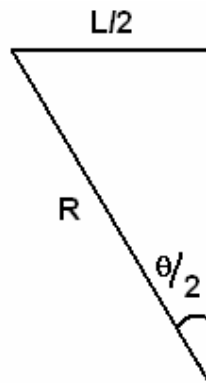


Figure 25 Relation between the angle and chord length

$$\sin \theta_1 / 2 = \frac{L/2}{R}$$

where $R = A / \theta$. Therefore we can write

$$L = \frac{A \sin(\theta/2)}{\theta/2} = A \text{sinc} \theta / 2\pi$$

Thus

$$\theta_1 = 2\pi \text{sinc}^{-1}\left(\frac{L_1}{A}\right) \text{ and } \theta_2 = 2\pi \text{sinc}^{-1}\left(\frac{L_2}{A}\right)$$

On the other hand

$$\Delta f_l = \theta_2 (R_2 + x) - \theta_1 (R_1 + x)$$

$$\Delta f_l = x(\theta_2 - \theta_1)$$

Substituting θ_1 and θ_2 we have

$$\Delta f_l = 2\pi x \left[\text{sinc}^{-1}\left(\frac{L_2}{A}\right) - \text{sinc}^{-1}\left(\frac{L_1}{A}\right) \right]$$

This length difference causes the grating spacings to increase, which in turn causes the central wavelengths of the FBGs to shift, enabling us to select different wavelengths.

Figure 26 shows the spectra of the three FBGs before any stretching is done. Filter peaks are at 1541,4nm, 1543nm and 1544.6 nm before applying stress. The peak values for this case are -42.2dBm, for the peak at 1546nm, -44.3dBm for the peak at 1548nm and -45.6dBm for the peak at 1550nm. Figure 27 shows the spectra after 5 turns of the screw. The peaks are now at 1540nm, 1541,4nm and 1543 nm. As seen from the graph, 5 turns of the screw is enough to move the spectrum from one peak

to the next, which is around 1.5nm. This enables us to choose any comb peak in between FBG peaks. The graphs are obtained with the FBG setup connected to a broadband source operating at 8mW total power. Changing the central wavelengths of FBGs by applying stress does not affect their peak values therefore peak values are same for both figures.

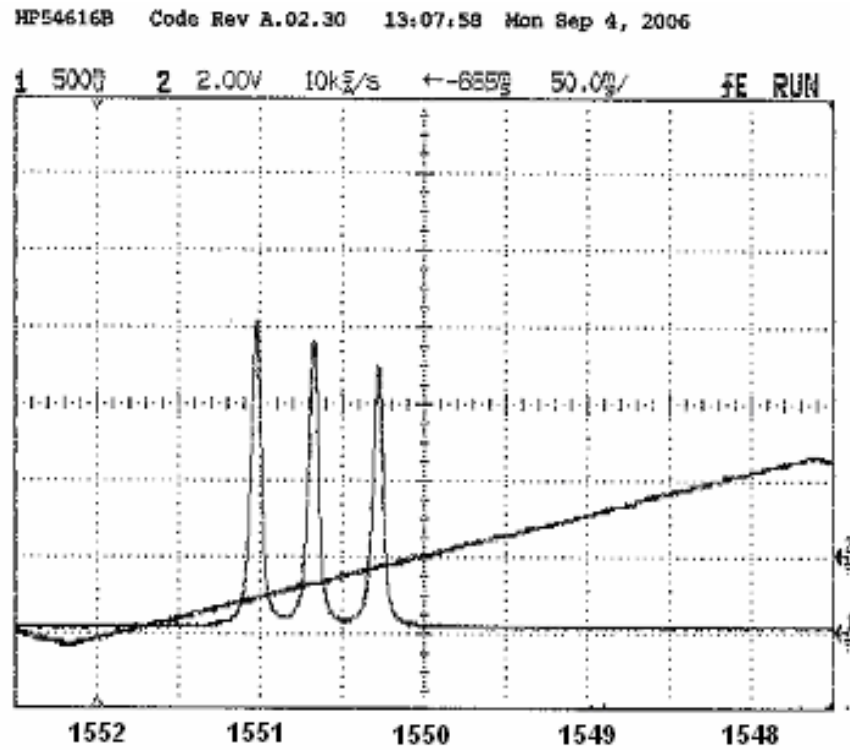


Figure 26 The spectrum of the FBGs before and stress is applied

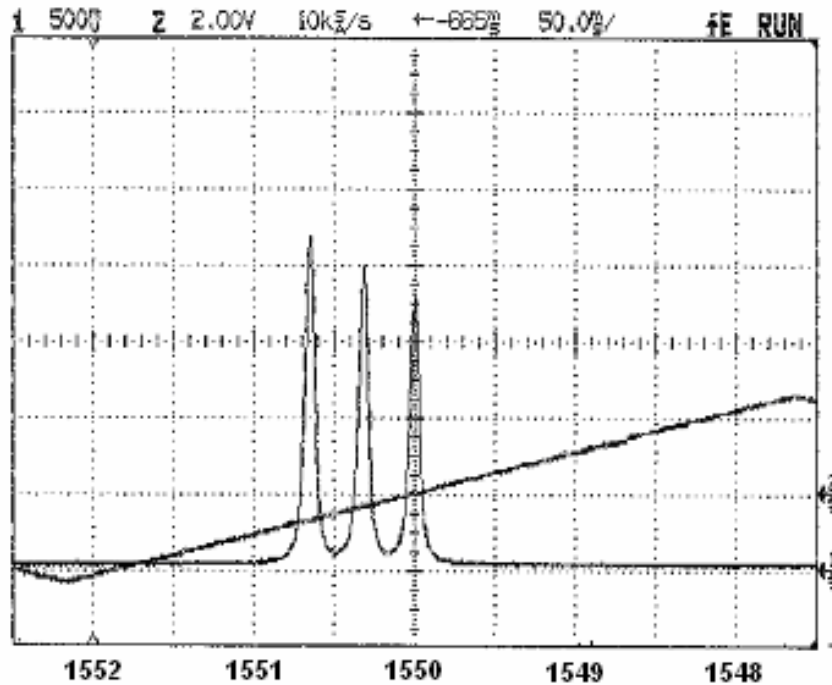


Figure 27 The spectrum of the FBGs after 5 turns of the screw

Lasing occurs at the wavelengths where the central wavelength of one or more of the FBGs coincides with the channel(s) provided by the Sagnac filter. With three FBGs in the adjustable filter configuration, up to three wavelengths can be produced by the source. Figure 28, Figure 29 and Figure 30 show single, dual and triple channel output of our source with doubly clad PM. Figure 31 and Figure 32 show single and dual channel output with the PANDA PM fiber. The peak for single channel operation is -3.5dBm, whereas the largest peaks for double and triple channel operation are -8.9dBm and -22.4dBm respectively for the doubly clad PM. For the PANDA PM, the peak for single channel output is -3.8dB, and the largest peak for dual channel operation is -22.1dB. Triple channel operation was not observed for the PANDA fiber within the region that the adjustable FBG setup can cover. This is most probably due to non-existence of a triple intersection between the PANDA PM Sagnac loop comb and the FBGs in the adjustable filter setup. It can be said that since the loop with the doubly clad PM has closer peaks, its

“resolution” is better compared to the loop with the PANDA fiber, increasing the chance of a triple intersection between loop peaks and the FBG peaks.

It should be noted that the double and especially triple channel operation is not very stable. This instability is due to the fact that without any temperature stabilizing the comb filter output has a certain drift. Since lasing occurs at the intersection points of the comb output and FBG center wavelengths, dual and triple channel operation requires more stability. A little drift in the frequency pattern may be enough to upset the balance of power established for a dual or triple channel operation. This causes power to shift from one lasing point to the other and back for two and three wavelength operation causing instability.

The spec sheets of all components used in both the fiber laser setup and the OSA setup can be found in Appendix E.

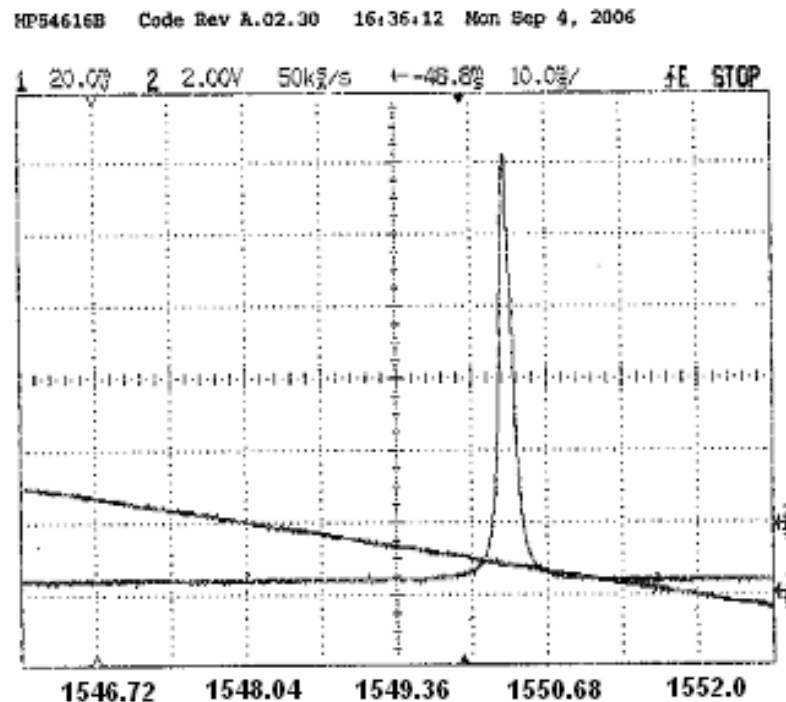


Figure 28 Single channel output of the source with doubly clad PM

HP54616B Code Rev A.02.30 16:37:08 Mon Sep 4, 2006

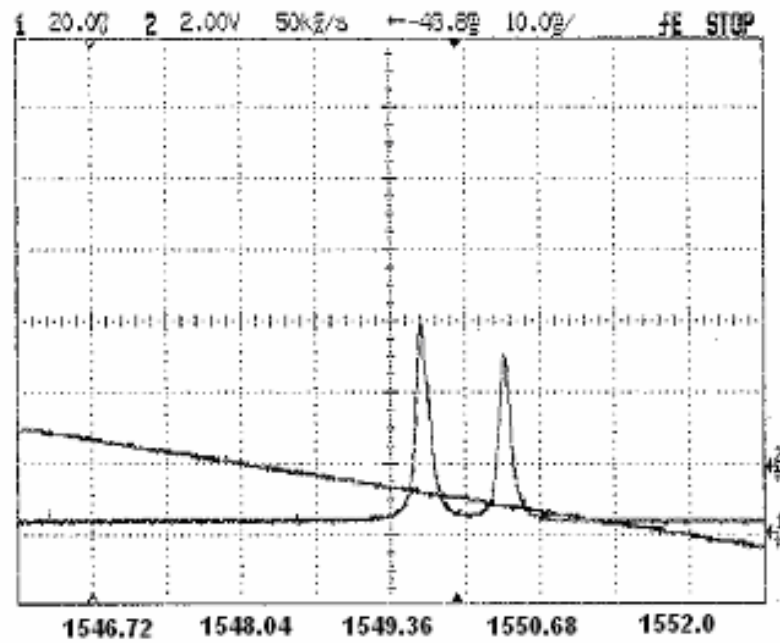


Figure 29 Dual channel output of the source with doubly clad PM

HP54616B Code Rev A.02.30 16:08:20 Mon Sep 4, 2006

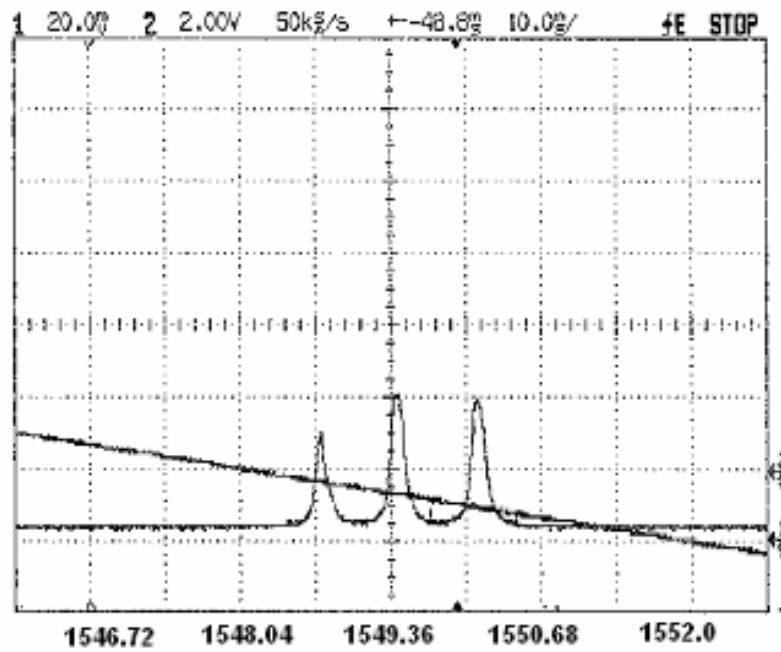


Figure 30 Three wavelength output of the source with doubly clad PM

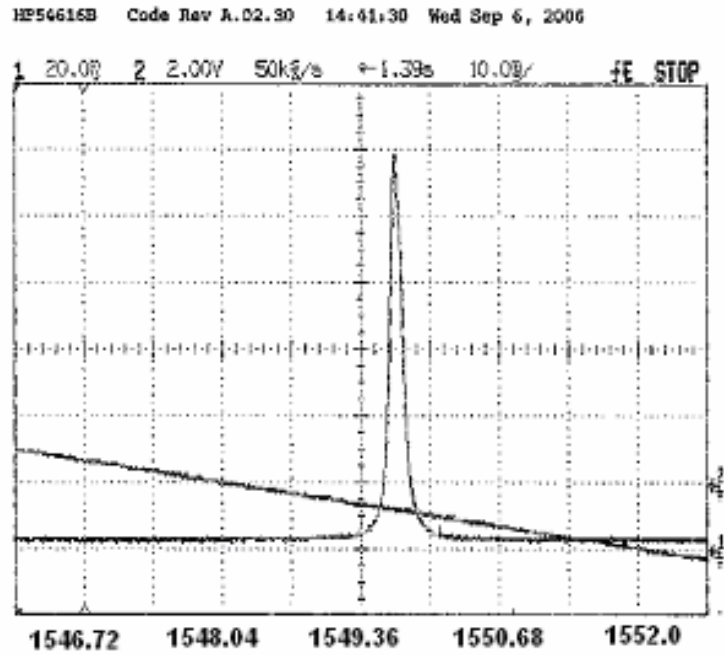


Figure 31 Single channel output with PANDA PM

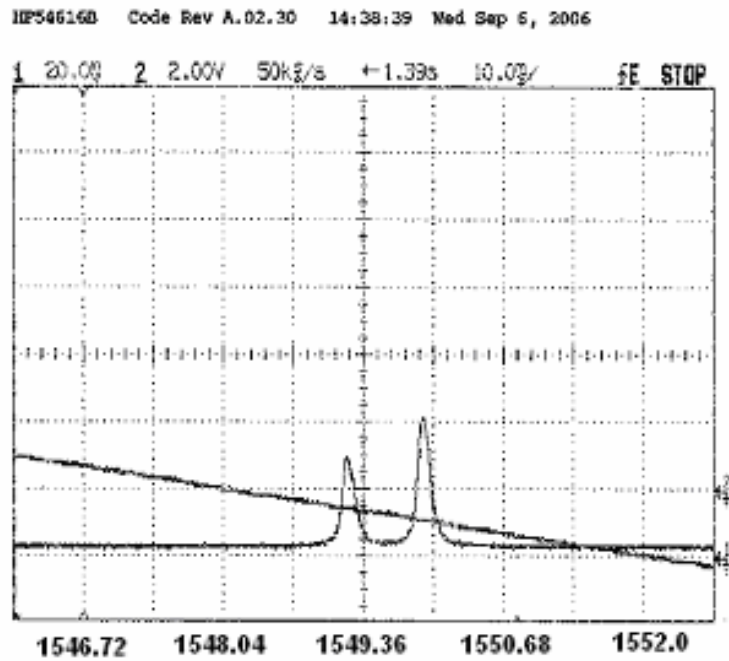


Figure 32 Dual channel output with PANDA PM

CHAPTER 5

CONCLUSION

This thesis presented a wavelength-selectable all-fiber laser source for WDM systems. The source utilizes a fiber Sagnac loop filter as a comb filter to produce a set of wavelengths. Then an adjustable FBG setup is used to select the desired “channel”.

We used two kinds of high birefringence PM fibers in the fiber Sagnac loop filter. The loop with PANDA PM fiber provided a peak to valley ratio of about 9 dB and the loop with doubly clad PM fiber provided a peak to valley ratio of 8dB on their grid outputs. One of the key factors determining this peak to valley ratio is the loss in the splices between the normal fiber of the coupler and the PM fiber that make up the loop of the Sagnac filter. Since PM fibers have non-standard core or cladding structures or have stress inducing regions between the core and the cladding, splicing a PM fiber with a normal fiber generally causes up to a few dB loss. In our lab we use a fusion splicer that can test the splice by coupling light into one of the fibers and measuring it from the other fiber. The splicing losses reported by the fusion splicer for the four normal fiber to PM fiber splices used in two Sagnac loops were between 0.7dB to 1.2dB. As a comparison, the common splicing loss we see with our fusion splicer when splicing two standard telecom fibers is around 0.04dB.

Another determining factor for the peak to valley ratio is the balance of the splicing losses. If the difference between the losses of the splices at one end of the loop and

the other is too big, the counterpropagating waves are no longer identical. Therefore the interference pattern they form when they meet again at the coupler is far from the ideal case. The net effect is a reduction in peak to valley ratio of the produced wavelength comb output.

The doubly clad PM fiber is specially manufactured for reduced splicing losses. It has a high core to cladding concentricity thus the cross section is not very different from a standard fiber. However in our many attempts to get better splicing results we didn't notice a significant difference between the doubly clad fiber and the PANDA fiber. In fact we obtained slightly better results for the PANDA PM fiber, and thus the peak to valley ratio for the loop that used PANDA fiber is 1dB better than the other loop.

Another important issue to note is the temperature dependence of the birefringence of these PM fibers. As we stated in chapter 3, birefringence depends on the temperature of the medium. Since the filter peak spacings of the Sagnac filter is a function of birefringence of the PM fiber used, as the temperature changes we see a "drift" in the set of wavelengths produced by the Sagnac filter. The temperature dependence of doubly clad PM fiber is expected to be lower than that of the PANDA fiber, since its thicker cladding helps in isolating the fiber from the outside effects like temperature changes. Although these drifts were too irregular to make any meaningful measurements we observed that the doubly clad PM was indeed more resistant to temperature changes than the PANDA PM fiber.

Even though temperature changes cause wavelength drifts at the Sagnac loop filter output, these wavelength drifts are not directly carried to the overall source output. The FBGs at the second stage of the filtering setup are highly resistant to temperature changes. Thus they somehow cancel this wavelength drift effect. However if the drift is too big, the peaks of the grid filter move too far away from their original position causing another peak to coincide with the central wavelength of another FBG in the BFG chain. This causes the wavelength of the source output to "jump" abruptly from one wavelength to another or change the output from single channel to two or three channel output or vice versa.

These drifts proved to be problematic especially for two and three channel operation where the lasing power is divided among channels. For these operations balancing the lasing power between channels is essential. The closed loop structure tends to amplify any unbalance rapidly causing one of the channels to be dominant and suppressing the other. Thus two and three channel operation is not reliable without further temperature stabilization to avoid comb filter output drifts.

For a single channel operation, the maximum output of the laser is measured to be around -3.5 dBm. The two and three channel outputs have much lower peak intensity values, because total power is shared between the channels. These output peak powers are lower than expected values. This is due to the high coupler to PM splice losses, losses at the connectors, the unavoidable 3dB return loss at the 50/50 coupler, and the insertion losses at the circulator, WDM and output couplers.

In conclusion, a wavelength selectable all fiber source that uses a fiber Sagnac loop filter with successful wavelength switching with single, dual and triple channel outputs have been demonstrated. The future work to improve the source further may include experimenting on various methods to reduce temperature dependence, hence improving long-term stability. Another issue to address is the high insertion losses. To reduce these losses all connectors may be replaced by fusion splices. Also a second stage amplification may be considered to increase the output power of the laser.

APPENDIX A

NORMALIZED JONES AND MUELLER VECTORS FOR LIGHT WITH VARIOUS SOP

	Normalized Jones Vectors	Normalized Stokes Vectors
Linear horizontally polarized light	$\begin{bmatrix} 1 \\ 0 \end{bmatrix}$	$\begin{bmatrix} 1 \\ 1 \\ 0 \\ 0 \end{bmatrix}$
Linear vertically polarized light	$\begin{bmatrix} 0 \\ 1 \end{bmatrix}$	$\begin{bmatrix} 1 \\ -1 \\ 0 \\ 0 \end{bmatrix}$
Linear 45° polarized light	$\frac{1}{\sqrt{2}} \begin{bmatrix} 1 \\ 1 \end{bmatrix}$	$\begin{bmatrix} 1 \\ 0 \\ 1 \\ 0 \end{bmatrix}$
Linear -45° polarized light	$\frac{1}{\sqrt{2}} \begin{bmatrix} 1 \\ -1 \end{bmatrix}$	$\begin{bmatrix} 1 \\ -1 \\ 0 \\ 0 \end{bmatrix}$

Right circularly polarized light	$\frac{1}{\sqrt{2}} \begin{bmatrix} 1 \\ -j \end{bmatrix}$	$\begin{bmatrix} 1 \\ 0 \\ 0 \\ 1 \end{bmatrix}$
----------------------------------	--	--

Left circularly polarized light	$\frac{1}{\sqrt{2}} \begin{bmatrix} 1 \\ j \end{bmatrix}$	$\begin{bmatrix} 1 \\ 0 \\ 0 \\ -1 \end{bmatrix}$
---------------------------------	---	---

APPENDIX B

MUELLER MATRICES FOR VARIOUS POLARIZERS AND RETARDERS

Mueller matrix for a polarizer at angle θ

$$\frac{1}{2} \begin{bmatrix} 1 & \cos 2\theta & \sin 2\theta & 0 \\ \cos 2\theta & \cos^2 2\theta & \cos 2\theta \sin 2\theta & 0 \\ \sin 2\theta & \cos 2\theta \sin 2\theta & \sin^2 2\theta & 0 \\ 0 & 0 & 0 & 1 \end{bmatrix}$$

Mueller matrix for a horizontal polarizer

$$\frac{1}{2} \begin{bmatrix} 1 & 1 & 0 & 0 \\ 1 & 1 & 0 & 0 \\ 0 & 0 & 0 & 0 \\ 0 & 0 & 0 & 0 \end{bmatrix}$$

Mueller matrix for a vertical polarizer

$$\frac{1}{2} \begin{bmatrix} 1 & -1 & 0 & 0 \\ -1 & 1 & 0 & 0 \\ 0 & 0 & 0 & 0 \\ 0 & 0 & 0 & 0 \end{bmatrix}$$

Mueller matrix for a linear polarizer at 45°

$$\frac{1}{2} \begin{bmatrix} 1 & 0 & 1 & 0 \\ 0 & 0 & 0 & 0 \\ 1 & 0 & 1 & 0 \\ 0 & 0 & 0 & 0 \end{bmatrix}$$

Mueller matrix for a right circular polarizer

$$\frac{1}{2} \begin{bmatrix} 1 & 0 & 0 & 1 \\ 0 & 0 & 0 & 0 \\ 0 & 0 & 0 & 0 \\ 1 & 0 & 0 & 1 \end{bmatrix}$$

Mueller matrix for a left circular polarizer

$$\frac{1}{2} \begin{bmatrix} 1 & 0 & 0 & -1 \\ 0 & 0 & 0 & 0 \\ 0 & 0 & 0 & 0 \\ -1 & 0 & 0 & 1 \end{bmatrix}$$

Mueller matrix for a linear retarder with fast axis at angle θ and retardation δ

$$\begin{bmatrix} 1 & 0 & 0 & 0 \\ 0 & \cos^2 2\theta + \sin^2 2\theta \cos \delta & (1 - \cos \delta) \sin 2\theta \cos 2\theta & -\sin 2\theta \sin \delta \\ 0 & (1 - \cos \delta) \sin 2\theta \cos 2\theta & \sin^2 2\theta + \cos^2 2\theta \cos \delta & \cos 2\theta \sin \delta \\ 0 & \sin 2\theta \sin \delta & -\cos 2\theta \sin \delta & \cos \delta \end{bmatrix}$$

Mueller matrix for a linear quarter wave retarder with fast axis at 0°

$$\begin{bmatrix} 1 & 0 & 0 & 0 \\ 0 & 1 & 0 & 0 \\ 0 & 0 & 0 & 1 \\ 0 & 0 & -1 & 0 \end{bmatrix}$$

Mueller matrix for a linear quarter wave retarder with fast axis at 45°

$$\begin{bmatrix} 1 & 0 & 0 & 0 \\ 0 & -1 & 0 & 0 \\ 0 & 0 & 1 & 0 \\ 0 & 0 & 0 & -1 \end{bmatrix}$$

APPENDIX C

JONES MATRICES FOR VARIOUS POLARIZERS AND RETARDERS

Jones matrix for linear polarizer at 0°

$$\begin{bmatrix} 1 & 0 \\ 0 & 0 \end{bmatrix}$$

Jones matrix for linear polarizer at 45°

$$\frac{1}{2} \begin{bmatrix} 1 & 1 \\ 1 & 1 \end{bmatrix}$$

Jones matrix for right circular polarizer

$$\frac{1}{2} \begin{bmatrix} 1 & j \\ -j & 1 \end{bmatrix}$$

Jones matrix for left circular polarizer

$$\frac{1}{2} \begin{bmatrix} 1 & -j \\ j & 1 \end{bmatrix}$$

Jones matrix for a retarder at angle θ

$$\begin{bmatrix} \cos^2 \theta & \cos \theta \sin \theta \\ \cos \theta \sin \theta & \sin^2 \theta \end{bmatrix}$$

Jones matrix for a linear retarder with fast axis at angle θ and retardation δ

$$\begin{bmatrix} e^{j\delta} \cos^2 \theta + \sin^2 \theta & (e^{j\delta} - 1) \cos \theta \sin \theta \\ (e^{j\delta} - 1) \cos \theta \sin \theta & e^{j\delta} \sin^2 \theta + \cos^2 \theta \end{bmatrix}$$

Jones matrix for a quarter wave retarder with fast axis at 0°

$$\begin{bmatrix} e^{j\pi/4} & 0 \\ 0 & e^{-j\pi/4} \end{bmatrix}$$

Jones matrix for a half wave retarder with fast axis at 45°

$$\begin{bmatrix} 0 & 1 \\ 1 & 0 \end{bmatrix}$$

APPENDIX D

RELATIONSHIPS BETWEEN MUELLER AND JONES MATRIX ELEMENTS

Mueller matrix elements in terms of Jones matrix elements:

$$\begin{aligned}m_{11} &= (j_{11}j_{11}^* + j_{12}j_{12}^* + j_{21}j_{21}^* + j_{22}j_{22}^*)/2 \\m_{12} &= (j_{11}j_{11}^* + j_{12}j_{12}^* - j_{21}j_{21}^* - j_{22}j_{22}^*)/2 \\m_{13} &= (j_{12}j_{11}^* + j_{22}j_{21}^* + j_{11}j_{12}^* + j_{21}j_{22}^*)/2 \\m_{14} &= j(j_{12}j_{11}^* + j_{22}j_{21}^* - j_{11}j_{12}^* - j_{21}j_{22}^*)/2\end{aligned}$$

$$\begin{aligned}m_{21} &= (j_{11}j_{11}^* + j_{12}j_{12}^* - j_{21}j_{21}^* - j_{22}j_{22}^*)/2 \\m_{22} &= (j_{11}j_{11}^* - j_{12}j_{12}^* - j_{21}j_{21}^* + j_{22}j_{22}^*)/2 \\m_{23} &= (j_{11}j_{12}^* + j_{12}j_{11}^* - j_{21}j_{22}^* + j_{22}j_{21}^*)/2 \\m_{24} &= j(j_{12}j_{11}^* + j_{21}j_{22}^* - j_{22}j_{21}^* - j_{11}j_{12}^*)/2\end{aligned}$$

$$\begin{aligned}m_{31} &= (j_{11}j_{22}^* + j_{21}j_{11}^* + j_{12}j_{22}^* + j_{22}j_{12}^*)/2 \\m_{32} &= (j_{11}j_{21}^* - j_{21}j_{11}^* - j_{12}j_{22}^* - j_{22}j_{12}^*)/2 \\m_{33} &= (j_{11}j_{22}^* + j_{12}j_{21}^* + j_{21}j_{12}^* + j_{22}j_{11}^*)/2 \\m_{34} &= j(-j_{11}j_{22}^* + j_{12}j_{21}^* - j_{21}j_{12}^* + j_{22}j_{11}^*)/2\end{aligned}$$

$$\begin{aligned}m_{41} &= j(j_{11}j_{21}^* + j_{12}j_{22}^* - j_{21}j_{11}^* - j_{22}j_{12}^*)/2 \\m_{42} &= j(j_{11}j_{21}^* - j_{12}j_{22}^* - j_{21}j_{11}^* + j_{22}j_{12}^*)/2 \\m_{43} &= j(j_{11}j_{22}^* + j_{12}j_{21}^* - j_{21}j_{12}^* - j_{22}j_{11}^*)/2 \\m_{44} &= (j_{11}j_{22}^* - j_{12}j_{21}^* - j_{21}j_{12}^* + j_{22}j_{11}^*)/2\end{aligned}$$

When Jones matrix elements are expressed in the form $j = r e^{j\theta}$ in terms of Mueller matrix elements they can be expressed as

$$r_{11} = \left[\frac{(m_{11} + m_{12} + m_{21} + m_{22})}{2} \right]^{1/2}$$

$$r_{12} = \left[\frac{(m_{11} - m_{12} + m_{21} - m_{22})}{2} \right]^{1/2}$$

$$r_{21} = \left[\frac{(m_{11} + m_{12} - m_{21} - m_{22})}{2} \right]^{1/2}$$

$$r_{22} = \left[\frac{(m_{11} - m_{12} - m_{21} + m_{22})}{2} \right]^{1/2}$$

$$\cos(\theta_{11} - \theta_{12}) = \frac{(m_{13} + m_{23})}{\left[(m_{11} + m_{21})^2 - (m_{12} + m_{22})^2 \right]^{1/2}}$$

$$\sin(\theta_{11} - \theta_{12}) = \frac{(m_{14} + m_{24})}{\left[(m_{11} + m_{21})^2 - (m_{12} + m_{22})^2 \right]^{1/2}}$$

$$\cos(\theta_{21} - \theta_{22}) = \frac{(m_{31} + m_{32})}{\left[(m_{11} + m_{12})^2 - (m_{21} + m_{22})^2 \right]^{1/2}}$$

$$\sin(\theta_{11} - \theta_{12}) = \frac{(m_{41} + m_{42})}{\left[(m_{11} + m_{12})^2 - (m_{21} + m_{22})^2 \right]^{1/2}}$$

$$\cos(\theta_{11} - \theta_{22}) = \frac{(m_{33} + m_{44})}{\left[(m_{11} + m_{22})^2 - (m_{21} + m_{12})^2 \right]^{1/2}}$$

$$\sin(\theta_{22} - \theta_{11}) = \frac{(m_{43} + m_{34})}{\left[(m_{11} + m_{22})^2 - (m_{21} + m_{12})^2 \right]^{1/2}}$$

APPENDIX E

OPTICAL SPECTRUM ANALYZER SETUP

The picture of the optical spectrum analyzer setup is shown in Figure 33



Figure 33 A photo of the OSA setup

The bandwidth of the adjustable filter is very narrow (0.21 nm). Its central wavelength can be controlled by two methods. First is the analog voltage control input. A range between -5 volts and 5 volts corresponds to a shift between 1520 nm to 1560 nm of the central wavelength of the filter. Therefore by applying a ramp signal between certain voltages, one can make the filter scan a certain wavelength range.

The second way to control the central wavelength is via the 14-pin digital control input. A bit pattern of 00000000000000 sets the central wavelength to 1520nm and a bit pattern of 11111111111111 sets the central wavelength to 1560nm. A digital up/down counter circuit is constructed on a protoboard to be able to make the filter scan a wavelength range using the digital control input. By setting limiting bit patterns using an upper and a lower limit switch one can control the range that the counter will span.

Two binary up/down counters (74LS193) are cascaded to obtain a 14-bit counter. Similarly two 8-bit magnitude comparators (74HC688) are cascaded to obtain a 14-bit comparator to compare the value at the upper and lower limit switches with the current value at the counter output. The comparator outputs are connected as an input to a J-K flip-flop (SN7470). A change in the output value of the comparator causes a toggle at the output of the flip-flop. The output pins Q and \overline{Q} are connected to the up/down control of the counter, and thus causes the counter to start counting up or down depending on the exceeded limit. Since the up/down counter is connected to the digital control input of the filter, the range set for the up/down counter determines the maximum and minimum wavelengths that the filter will scan. Figure 34 shows the block diagram and Figure 35 shows a photograph of the up/down counter.

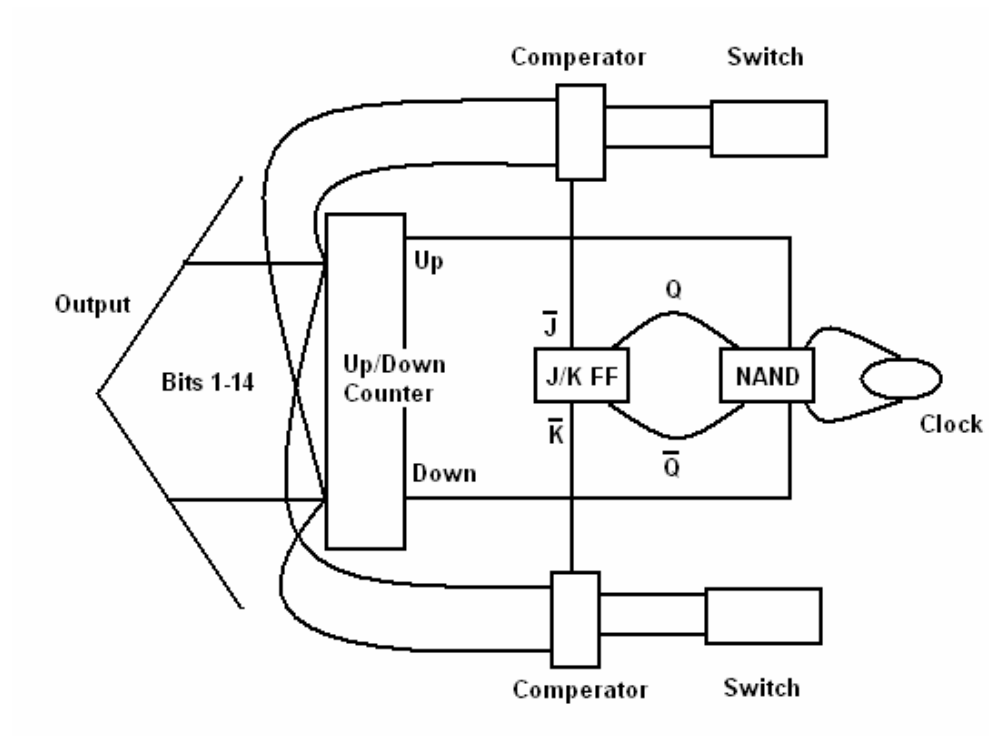


Figure 34 The block diagram of the up/down counter

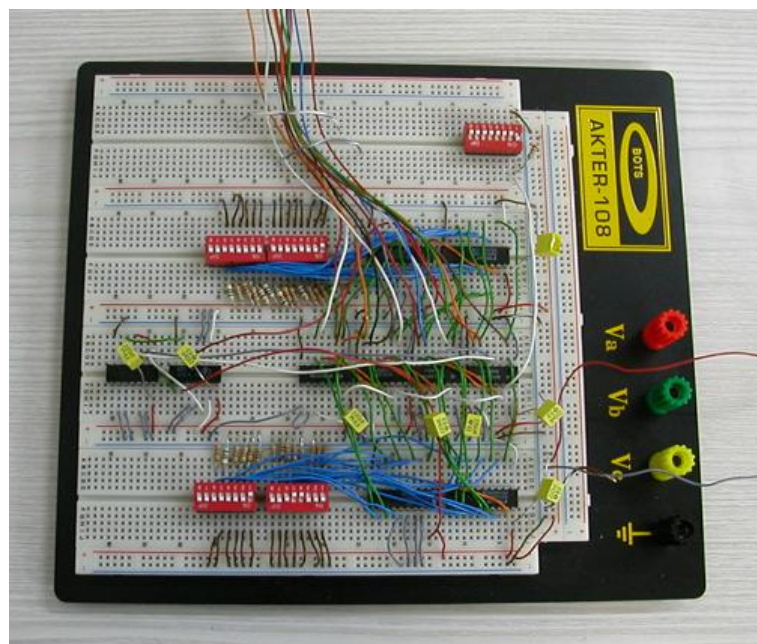


Figure 35 A photo of the up/down counter



The output of the filter is sent to the optical powermeter, which measures the optical intensity. The powermeter has a wavelength range of 800-1700 nm and a power range of +3 to -110dBm. Its display resolution is 0.001dBm, 0.001dB or 0.01pW with an uncertainty of $\pm 2.5\%$. The analog output of the optical powermeter can be used to obtain an electrical signal proportional to the intensity of the light at the powermeter's input. This electrical signal is fed into the oscilloscope. The filter scans a certain wavelength range in time as the oscilloscope traces the screen, so that at a certain time oscilloscope traces the intensity of the light at the wavelength that the filter's center is located at that moment. That's why the x-axis of the oscilloscope in fact becomes wavelength axis, while the y-axis indicates the intensity of the light at that wavelength. The filter can scan a 30 nm range at 2Hz. Overall this setup gives us a very good optical spectrum analyzer at a very low price, which has finesse and sensitivity that is higher than standard, commercially available optical spectrum analyzers.

APPENDIX F

THE SPEC SHEETS OF THE COMPONENTS USED IN THE FIBER LASER SETUP

The spec sheet for the 3dB coupler used in the Sagnac loop filter with the doubly clad PM fiber


Product code	C-WD-AL-50-H-2210-35-NC/NC
Serial number	07009494
Operating wavelength (nm)	1310/1550 nm
Fiber type	SMF-28
Coupling ratio (%)	50.10 / Blue:50.70 %
Insertion loss (dB)	3.22/3.19 dB
Bandwidth (nm)	± 40 nm
Directivity (dB)	60 dB
Return loss (dB)	55 dB
Polarization dependent loss (dB)	<0.1 dB
Thermal stability (dB)	<0.3 dB


	
Approved by : _____	

Patchcord / Pigtail / Parts / Adaptor / Coupler / WDM / Filter / Attenuator / Collimator / Isolator / Circulator / Converter

The spec sheet for the 3dB coupler used in the Sagnac loop filter with the PANDA PM fiber

Product code		C-WD-AL-50-H-2210-35-NC/NC
Serial number		07009463
Operating wavelength (nm)		1310/1550 nm
Fiber type		SMF-28
Coupling ratio (%)		49.20 / Blue:51.30 %
Insertion loss (dB)		3.39/3.31 dB
Bandwidth (nm)		±40 nm
Directivity (dB)		60 dB
Return loss (dB)		55 dB
Polarization dependent loss (dB)		<0.1 dB
Thermal stability (dB)		<0.3 dB







Approved by : _____

Patchcord / Pigtail / Parts / Adaptor / Coupler / WDM / Filter / Attenuator / Collimator / Isolator / Circulator / Converter

Spec sheet for the WDM coupler

Fiber Optic Wavelength Division Multiplexer	
Product code	W-PM-BL-XX-1-1210-95-NC/NC
Serial number	00052123
Fiber type	Coming Flexcor
Wavelength range (λ_1/λ_2) (nm)	Red:980/Blue:1550
Insertion loss (λ_1/λ_2) (dB)	0.21 dB/0.16 dB
Insertion loss (over specified bandwidth) (dB)	-
Isolation (center wavelength) (dB)	24.79 dB
Isolation (over specified bandwidth) (dB)	-
Bandwidth (nm)	±10 nm
Directivity (dB)	62.83 dB
Thermal stability (dB)	<0.2 dB
Polarization dependent loss (dB)	<0.1 dB





Please refer reverse page for more informations

Approved by : _____

Patchcord / Pigtail / Parts / Adaptor / Coupler / WDM / Filter / Attenuator / Collimator / Isolator / Circulator / Grating / Instruments

Spec sheet for the circulator

Test Data

Name: CIRCULATOR

Model: CTR-3-155-A-09-1-7C/PC S/N: 113165

Specifications

Wavelength Range		nm	1525 - 1575
Insertion Loss	1→2	dB	0.71
	2→3		0.63
Isolation	2→1	dB	53
	3→2		50
Directivity	1→3	dB	58
	3→1		68
Return Loss	1	dB	53
	2		53
	3		54
PDL	1→2	dB	0.05
	2→3		0.15
PMD		ps	<0.05
Operating Temperature	°C		0 to +70
Storage Temperature	°C		-40 to +85

Tested By: Hix Test Date: 8-10-04

The spec sheet for the isolator



435 Route 206 • P.O. Box 366
Newton, NJ 07860-0366

Ph: 973-679-7227

FAX 973-383-8406

4013SA/4015SA
POLARIZATION INSENSITIVE SINGLE
STAGE FIBEROPTIC ISOLATER

The Thorlabs Polarization Insensitive Single Stage Fiberoptic Isolator is a passive, non-reciprocal, high performance lightwave component for suppressing optical feedback in laser-based fiberoptic systems. The component provides very low insertion loss, high isolation, high return loss, and excellent environmental stability and reliability in a compact rugged package.

SPECIFICATIONS:

Center Wavelength:	1310 or 1550nm
Typical Peak Isolation	>40dB
Minimum Isolation	>32dB
(Over the center wavelength +/-15nm, at 23 degrees C, all polarization states)	
Typical Insertion Loss	0.4dB
(Over the center wavelength +/-20nm, at 23 degrees C, all polarization states)	
Maximum Insertion Loss	<0.7dB
(Over the center wavelength +/-20nm, at -20 degrees C to +60 degrees C, all polarization states)	
Return Loss (Input/Output)	>65/60dB
PDL	<0.1dB
PMD	<0.25*ps
Maximum Optical Power	300mW
Maximum Tensile	5N
Operating Temperature	-20 to +60 degrees C
Storage Temperature	-40 to +85 degrees C
Fiber Length	1m

*PMD <0.05 ps version is available.

The spec sheet for the filter used in the OSA setup



Queensgate Instruments Ltd

Waterside Park, Bracknell,
Berkshire, RG12 1RB,
England

Tel: 01344 484111
Fax: 01344 484115
E-mail qi@queensgate.com

QUEENSGATE MicroFilter CALIBRATION DATA SHEET

Parameter	Value	Units
Filter Type	DMF300C	
Filter Serial Number	1240	
Controller Serial Number	48410	
Insertion Loss	3.36	dB
-3dB Bandwidth	0.21	nm
-20dB Bandwidth	2.50	nm
FSR	41.25	nm
Finesse	196	
Return Loss	23.5	dB



Certified to ISO 9001
Registered Office
Queensgate House,
Waterside Park,
Bracknell, Berkshire,
RG12 1RB, England
Registered No 1415493
England

The first page of the spec sheet of the pump laser of the EDFA.

2600-TE Series Pumps | 3

Table 1: Absolute Maximum Ratings

Parameter	Symbol	Test Condition	Minimum	Maximum
Operating case temperature	T_{op}	-	-20 °C	75 °C
Storage temperature	T_{stg}	2000 hours	-40 °C	85 °C
LD submount temperature	T_{LD}	-	0 °C	50 °C
LD reverse voltage	V_r	-	-	2 V
LD forward current	-	-	-	650 mA
LD current transient	-	1 μ s maximum	-	950 mA
LD reverse current	-	-	-	10 μ A
PD reverse voltage	V_{PD}	-	-	20 V
PD forward current	I_{FD}	-	-	10 mA
Electrostatic discharge (ESD)	V_{ESD}	C = 100 pF, R = 1.5 Ω , human body model	-	1000 V
TEC current	I_{TEC}	-	-	2.5 A
TEC voltage	V_{TEC}	-	-	4.0 V
Axial pull force	-	3 x 10 seconds	-	5 N
Side pull force	-	3 x 10 seconds	-	2.5 N
Fiber bend radius	-	-	16 mm	-
Relative humidity	R_H	40 °C	5%	95%
Lead soldering time	-	260 °C	-	10 seconds

Note: Absolute maximum ratings are the maximum stresses that may be applied to the pump module for short periods of time without causing damage. Stresses in excess of the absolute maximum ratings can permanently damage the device. Exposure to absolute maximum ratings for extended periods, or exposure to more than one absolute maximum rating simultaneously may adversely affect device reliability.

Table 2: Operating Parameters (BOL, $T_{amb} = 0$ to 75 °C, $T_{LD} = 25$ °C, -50 dB reflection, unless noted otherwise)

Product Code ¹	Maximum Operating Power P_{op} (mW) ^{2,3}	Maximum Operating Current I_{op} (mA)	Minimum Kink-Free Power P_{min} (mW) ⁴	Kink-Free Current I_{max} (mA) ³
	Maximum ²		Maximum ⁴	
26-xxxx-100-TE	90	240	100	260
26-xxxx-110-TE	100	240	110	260
26-xxxx-120-TE	110	260	120	270
26-xxxx-130-TE	120	270	130	290
26-xxxx-140-TE	125	280	140	310
26-xxxx-150-TE	135	300	150	330
26-xxxx-160-TE	145	320	160	350
26-xxxx-170-TE	155	340	170	370
26-xxxx-180-TE	160	340	180	380

- The 27-xxxx-xxx-TE may be substituted for this part series. All 26-xxxx-xxx-TE end product specifications will remain as published; there is no change to part numbers, product testing, quality or reliability. Traceability is accomplished through product serial number.
- The maximum operating power P_{op} will be achieved at a device-specific current, the maximum operating current I_{op} . The individual value of I_{op} is noted on the hardcopy data sheet shipped with the device. All values of I_{op} are limited by the maximum value listed in Table 2.
- The pump laser shall never be operated at a power higher than the maximum operating power P_{op} throughout its lifetime. At *Begin of Life* (BOL), the operating current shall never be higher than the device-specific maximum operating current I_{op} that is noted on the hardcopy data sheet shipped with the device. At *End of Life* (EOL), the operating current shall never be higher than the device-specific kink-free current I_{max} that is noted on the hardcopy data sheet shipped with the device.
- The module is kink-free (at least) up to a minimum kink-free power P_{min} that the module will achieve at a device-specific current, the kink-free current I_{min} . The individual value of I_{min} is noted on the hardcopy data sheet shipped with the device. All values of I_{min} are limited by the maximum value listed in Table 2.

The second page of the spec sheet of the pump laser of the EDFA.

2600-TE Series Pumps | 4

Table 3: Available Peak Wavelength Selection ($T_{amb} = 25 \pm 3^\circ\text{C}$, $50 \text{ mW} < P < P_{op}$)

Product Code	Minimum Peak Wavelength	Maximum Peak Wavelength
26-8000-xxx-TE	970.0 nm	985.0 nm
26-7402-xxx-TE	973.0 nm	975.0 nm
26-7552-xxx-TE	974.5 nm	976.5 nm
26-7602-xxx-TE	975.0 nm	977.0 nm
26-7702-xxx-TE	976.0 nm	978.0 nm
26-8052-xxx-TE	979.5 nm	981.5 nm

Table 4: Electro-Optical Performance (BOL, $T_{amb} = 0$ to 75°C , $T_{LH} = 25^\circ\text{C}$, -50 dB reflection, unless noted otherwise)

Parameter	Symbol	Test Condition	Minimum	Maximum
Threshold current	I_{th}	-	-	25 mA
Forward voltage	V_f	$I_f = I_{op}$	-	2.5 V
Spectral width	$\Delta\lambda_{RMS}$	$50 \text{ mW} < P < P_{op}$	-	2.0 nm
Peak wavelength tuning	$\Delta\lambda_p / \Delta T_{amb}$	$50 \text{ mW} < P < P_{op}$	-	0.02 nm/ $^\circ\text{C}$
Side-mode suppression ratio	SMSR	$50 \text{ mW} < P < P_{op}$	15 dB	-
Relative optical power stability		Peak-to-peak, $T = 10 \text{ min}$, 50 kHz sampling, $T_{amb} = 25^\circ\text{C}$		
		$20 \text{ mW} < P < P_{op}$	-	4%
		$12 \text{ mW} < P < 20 \text{ mW}$	-	10%
		$3.5 \text{ mW} < P < 12 \text{ mW}$	-	25%
Tracking error	TE	$20 \text{ mW} < P < P_{op}^1$	-8%	8%
Tracking ratio	TR	$20 \text{ mW} < P < P_{op}^2$	0.90	1.10
Monitor diode responsivity	Resp_{DF}	$20 \text{ mW} < P < P_{op}$	2 $\mu\text{A/mW}$	10 $\mu\text{A/mW}$
TEC current	I_{TEC}	$T_{amb} = 75^\circ\text{C}$	-	1.5 A
TEC voltage	V_{TEC}	$T_{amb} = 75^\circ\text{C}$	-	2.5 V
Thermistor resistance	R_{th}	-	9.5 k Ω	10.5 k Ω
Thermistor constant	B	-	3600 K	4200 K
Module power consumption		$T_{amb} = 75^\circ\text{C}$	-	4.5 W
Module power consumption		$T_{amb} = 75^\circ\text{C}$, EOL	-	5.5 W

1. The Tracking Error is defined as the normalized change of output power relative to the operating power over case temperature range 0°C to 75°C , at constant back face monitor current corresponding to the operating power at 25°C .

2. The Tracking Ratio is a measure of the front-to-back tracking when the output power is varied. On a plot of optical power versus back-face photocurrent, a straight line is drawn between the minimum power (20 mW) and the operating power Pop points. The tracking ratio is defined as the ratio between measured optical power (shown as data points on the plot) to the value derived from the straight line.

REFERENCES

- [1] ITU-T G.694.2 Spectral grids for WDM applications: CWDM frequency grid
- [2] ITU-T G.694.1 Spectral grids for WDM applications: DWDM frequency grid
- [3] V. Jayaraman, Z. M. Chuang, and L. Coldren, "Theory, design and performance of extended tuning range semicond. Lasers with sampled gratings," *IEEE J. Quantum Electron.*, pp. 1824-1834, June 1993
- [4] T. Day, "Small form factor tunable laser," in *Tech. Dig. Optical Fiber Communications*, Anaheim, CA, Mar. 2001, Paper TuJ4.
- [5] Nathaniel J. C. Libatique and Ravinder K. Jain, "A broadly tunable wavelength-selectable WDM source using a fiber Sagnac loop filter," *IEEE Photonics Tech. Lett.* Vol. 13, No. 12, pp. 1283-1285, December 2001
- [6] S. Hu, L. Zhan, Y. J. Song, W. Li., S. Y. Luo, and Y. X. Xia, "Switchable multiwavelength erbium-doped fiber ring laser with a multisection high-birefringence fiber loop mirror," *IEEE Photonics Tech. Lett.*, Vol. 17, No. 7, pp. 1387-1389, July 2005.
- [7] Stokes, G. G., "On Composition and resolution of streams of polarized light from different sources," *Trans. Cambridge Phil. Soc.*, **9**, 399-416, 1852
- [8] Jones, R. C. "A new calculus for the treatment of optical systems: I. Description and discussion of the calculus," *J. Opt. Soc. Am.*, **31**, 488-493, July 1941
- [9] Poincaré, H. "Concerning theoretical descriptions of polarized light," *Théorie mathématique de la lumière*, Georges Carré, ed., Paris, 1892, pp. 275-285
- [10] A. L. Schawlow, C. H. Townes, "Infrared and Optical Masers", *Physical Review*, Vol. 112, pp. 1940-1949, December 1958.
- [11] Dessurvire, Emmanuel, "Erbium-Doped Fiber Amplifiers Principles and Applications", John Wiley, New Jersey, 2002
- [12] A. Yariv, "Quantum electronics," second ed., John Wiley, New York, 1975.
- [13] A. E. Siegman, "Lasers", University Science Books, Mill Valley, CA, 1986.

- [14] W. Eickhoff and E. Brinkmeyer, "Scattering loss vs. Polarization holding ability of single-mode fibers," *Appl. Opt.*, **23**, pp. 1131-1132, 1984.
- [15] H. Schneider, H. Harms, A. Rapp and H. Aulich, "Low birefringence single-mode fibers: Preparation and polarization characteristics," *Appl. Opt.*, **17**(19), pp. 3035-3037, 1978.
- [16] S. R. Norman, D. N. Payne, M. J. Adams and A. M. Smith, "Fabrication of single-mode fibers exhibiting extremely low polarization birefringence," *Electron. Lett.*, **15**(11), pp 309-311, 1979.
- [17] J. Noda, K. Okamoto and Y. Sasai, "Polarization maintaining fibers and their applications," *J. of Lightwave Technol.*, **LT-4**(8), pp. 1071-1089, 1986.
- [18] J. N. Ross, "The rotation of polarization in low birefringence monomode fibers due to geometric effects," *Optical and Quantum Electronics*, vol. 16, pp. 455-461, 1984.
- [19] M. P. Varnham, R. D. Birch, and D. N. Payne, "Design of helical-core circularly birefringent fibers," *Proceedings of OFC 1986*, Atlanta, USA, p.68.
- [20] Kenneth O. Hill and Gerald Meltz, "Fiber Bragg Grating Technology Fundamentals and Overview," *J. of Lightwave Technol.*, **15**(8), August 1997.
- [21] X. Fang and R. O. Claus, "Polarization-independent all-fiber WDM based on a Sagnac interferometer," *Opt. Lett.*, vol 20, no. 20, pp.2146-2148, 1995.
- [22] Reinhard Ulrich, "Optical Fiber Rotation Sensing," edited by William K. Burns, Academic Press, 1994.